Pontifícia Universidade Católica
do Rio de Janeiro

Diana Marcela Viveros Melo

Advanced transmit processing for MIMO downlink channels with 1-bit quantization and oversampling at the receivers

Dissertação de Mestrado

Thesis presented to the Programa de Pós–graduação em Engenharia Elétricada PUC-Rio in partial fulfillment of the requirements for the degree of Mestre em Engenharia Elétrica.

Advisor: Prof. Lukas Tobias Nepomuk Landau

Rio de Janeiro
March 2020

Pontifícia Universidade Católica
do Rio de Janeiro

Diana Marcela Viveros Melo

Advanced transmit processing for MIMO downlink channels with 1-bit quantization and oversampling at the receivers

Thesis presented to the Programa de Pós–graduação em Engenharia Elétricada PUC-Rio in partial fulfillment of the requirements for the degree of Mestre em Engenharia Elétrica. Approved by the undersigned Examination Committee.

Prof. Lukas Tobias Nepomuk Landau
Advisor
Centro de Estudos em Telecomunicações (CETUC) – PUC-Rio

Prof. Tadeu Nagashima Ferreira
Universidade Federal Fluminense – UFF

Prof. Rodrigo Caiado de Lamare
Centro de Estudos em Telecomunicações (CETUC) – PUC-Rio

Prof. Marco Antonio Grivet Mattoso Maia
Centro de Estudos em Telecomunicações (CETUC) – PUC-Rio

Rio de Janeiro, March the 6th, 2020

Diana Marcela Viveros Melo

Majored in Electronical Engineering by the University of Narino (Pasto, Colombia).

Bibliographic data

Viveros Melo, Diana Marcela

Advanced transmit processing for MIMO downlink channels with 1-bit quantization and oversampling at the receivers / Diana Marcela Viveros Melo; advisor: Lukas Tobias Nepomuk Landau. – Rio de janeiro: PUC-Rio , Departamento de Centro de Estudos em Telecomunicações (CETUC), 2020.

v., 71 f: il. color. ; 30 cm

Dissertação (mestrado) - Pontifícia Universidade Católica do Rio de Janeiro, Departamento de Centro de Estudos em Telecomunicações (CETUC).

Inclui bibliografia

1. Engenharia Elétrica – Teses. 2. Sistemas de Comunicações – Teses. 3. Pré-codificação com cruzamento de zero;. 4. Quantização de 1 bit;. 5. Sistemas MIMO;. 6. Sinalização mais rápida que Nyquist;. 7. Sobreamostragem;. 8. Erro quadrático médio.. I. Landau, Lukas Tobias Nepomuk. II. Pontifícia Universidade Católica do Rio de Janeiro. Departamento de Centro de Estudos em Telecomunicações (CETUC). III. Título.

CDD: 620.11

To my mom, brother and sister for their support
and encouragement.

Acknowledgments

I would first like to thank my advisor professor Lukas Landau for trusting my abilities and providing me the opportunity to work with him. I am grateful to him for his support, guidance and always be willing to solve my doubts and show me the best way to carry out my research.

I want to thank the CETUC professors for sharing their knowledge and their accompaniment during these two years, especially professors Rodrigo de Lamare, Raimundo Sampaio Neto and Jose Mauro Pedro Fortes. I am also grateful to the members of my defense committee, professor Rodrigo de Lamare, professor Tadeu N. Ferreira and professor Marco Antonio Grivet, who generously took their time to evaluate my thesis.

I had the opportunity to share a laboratory with wonderful people. I want to thank David and Dayrene for the time of study that we shared together and for their friendship and collaboration. Thanks to my Brazilian colleagues Erico and Victoria for their kindness and to my great friend Alireza for teaching me about his culture and also to my colleagues Pastusos Jose and Juan Pablo for their support and friendship.

I want to thank those people with whom we share special times, that even being far from my country who made me feel at home and they became my family. Among them my great friend Fabian for always taking care of me, and my other friends Alberth, Freddy, Lucas, Priscila, Alison, Andres, Esteban and Jorge. I want to give special thanks to Mrs. Lucia for opening the doors of her home to me.

I want to thank God for leading me and to my mother Sandra, my brother Andres and my sister Viviana for being my strength in this process and I also want to thank my boyfriend John for his love, support, and patience.

I want to give a special thanks to my friend, professor Diego Peluffo and the SDAS research group for their support and motivation. Finally, I want to thank the government of Brazil and CNPq for financial support to complete my master's degree. This study was financed in part by the Coordenação de Aperfeiçoamento de Pessoal de Nível Superior - Brasil (CAPES) - Finance Code 001.

Abstract

Viveros Melo, Diana Marcela; Landau, Lukas Tobias Nepomuk (Advisor). **Advanced transmit processing for MIMO downlink channels with 1-bit quantization and oversampling at the receivers**. Rio de Janeiro, 2020. 71p. Dissertação de mestrado – Departamento de Centro de Estudos em Telecomunicações (CETUC), Pontifícia Universidade Católica do Rio de Janeiro.

The IoT refers to a system of interrelated computing devises which aims to transfer data over a network without requiring human-to-human or human-to-computer interaction. This Modern communication systems demand restrictions of low energy consumption and low complexity in the receiver. In this sense, the analog-to-digital converter represents a bottleneck for the development of the applications of these new technologies since it has a high energy consumption due to its high resolution. The research carried out concerning to the analog-to-digital converters with coarse quantization has shown that such devices are promising for the design of future communication systems. To balance the loss of information, due to the coarse quantization, the resolution in time is increased through oversampling. This thesis considers a system with 1-bit quantization and oversampling at the receiver with a bandlimited multiuser MIMO downlink channel and introduces, as the main contribution, the novel zero-crossing modulation which implies that the information is conveyed within the time instant of the zero-crossings. This method is used for the temporal precoding through the waveform design optimization for two different precoders, the temporal maximization of the minimum distance to the decision threshold with spatial zero forcing and the space-time MMSE precoding. The simulation results show that the proposed zero-crossing approach outperforms the state-of-the-art in terms of the bit error rate for both precoders studied. In addition, this novel modulation reduces the computational complexity, allows very low complexity devices and saves band resources in comparison to the state-of-the-art method. Additional analyses show that the zero-crossing approach is beneficial in comparison to the state-of-the-art method in terms of greater minimum distance to the decision threshold and lower MSE for systems with band limitations. Moreover, it was devised a bit-mapping scheme for zero-crossing modulation, similar to Gray-coding to further reduce the bit error rate.

Keywords

Zero-crossing precoding; 1-bit quantization; MIMO systems; Faster-than-Nyquist signaling; Oversampling; Mean-square-error.

Resumo

Viveros Melo, Diana Marcela; Landau, Lukas Tobias Nepomuk. **Processamento avançado de transmissão para canais de downlink MIMO com quantização de 1 bit e superamostragem nos receptores** . Rio de Janeiro, 2020. 71p. Dissertação de Mestrado – Departamento de Centro de Estudos em Telecomunicações (CETUC), Pontifícia Universidade Católica do Rio de Janeiro.

IoT refere-se a um sistema de dispositivos de computação inter-relacionados que visa transferir dados através de uma rede sem exigir interação humano-humano ou humano-para-computador. Esses sistemas de comunicação modernos, exigem restrições de baixo consumo de energia e baixa complexidade no receptor. Nesse sentido, o conversor analógico-digital representa um gargalo para o desenvolvimento das aplicações dessas novas tecnologias, pois apresenta alto consumo de energia devido à sua alta resolução. A pesquisa realizada em relação aos conversores analógico-digitais com quantização grosseira mostrou que esses dispositivos são promissores para o projeto de futuros sistemas de comunicação. Para equilibrar a perda de informações, devido à quantização grosseira, a resolução no tempo é aumentada através da superamostragem. Esta tese considera um sistema com quantização de 1 bit e superamostragem no receptor com um canal de downlink MIMO multiusuário com banda ilimitada e apresenta, como principal contribuição, a nova modulação de cruzamento de zeros que implica que a informação é transmitida no instante de tempo zero-crossings. Este método é usado para a pré-codificação temporal através da otimização do design da forma de onda para dois pré-codificadores diferentes, a maximização temporal da distância mínima até o limiar de decisão com forçamento a zero espacial e a pré-codificação MMSE no espácio-temporal. Os resultados da simulação mostram que a abordagem de cruzamento de zeros proposta supera o estado da arte em termos da taxa de erro de bits para os dois pré-codificadores estudados. Além disso, essa nova modulação reduz a complexidade computacional, permite dispositivos de complexidade muito baixa e economiza recursos de banda em comparação com o método mais avançado. Análises adicionais mostram que a abordagem do cruzamento de zeros é benéfica em comparação com o método mais avançado em termos de maior distância mínima até o limiar de decisão e menor MSE para sistemas com limitações de banda. Além disso, foi desenvolvido um esquema de mapeamento de bits para modulação de cruzamento por zero, semelhante à codificação de Gray para reduzir ainda mais a taxa de erro de bits.

Palavras-chave

Pré-codificação com cruzamento de zero; Quantização de 1 bit; Sistemas MIMO; Sinalização mais rápida que Nyquist; Sobreamostragem; Erro quadrático médio.

Table of contents

List of figures

List of tables

My beautiful epigraph

Marie Curie, *Life is not easy for any of us. But what of that? We must have perseverance and above all confidence in ourselves. We must believe that we are gifted for something and that this thing must be attained.*

List of Abreviations

ADC – Analog-to-Digital Converter
AWGN – Additive White Gaussian Noise
BER – Bit Error Rate
BM – Backward Mapping
BS – Base station
DAC – Digital-to-Analog Converter
DFT – Discrete Fourier Transform
FM – Forward Mapping
FTN – Faster-Than-Nyquist
IBI – Inter-Block-Interference
IoT – Internet of Things
ISI – Inter-Symbol-Interference
MIMO – Multiple-Input Multiple-Output
MISO – Multiple-Input Single-Output
ML – Maximum Likelihood
MMDDT – Maximization of the Minimum Distance to the Decision Threshold
MSE – Mean Square Error
MMSE – Minimum Mean Square Error
PSD – Power Spectral Density
QCQP – Quadratically Constrained Quadratic Program
QPSK – Quadrature Phase Shift Keying
RC – Raised-cosine
RRC – Root-raised-cosine
SISO – Single-Input Single-Output
SNR – Signal-to-noise ratio
ZC – Zero-Crossing
ZF – Zero Forcing

1
Introduction

1.1
Motivation and context

The Internet of Things (IoT) is one of the new technologies that gives way to modern communication systems, whose most promising applications include smart homes, intelligent transportation, health care, smart grid and industrial automation [1, 2]. One of the fundamentals of this technology is the use of devices for a long time (about 10 years) with the same battery, being in this case the energy consumption, an important restriction.

The analog-to-digital converters (ADCs) with high resolution mean a high energy consumption, which is the reason why the ADCs with low resolution have attracted attention in the scientific field becoming a highly attractive research topic. This is not only because of the the low consumption of energy but also because it involves low complexity devices, which makes it promising for this type of technology.

It is known that it is possible to increase the sampling rate at the receiver with a cost that is proportional to the sampling rate. With this, it is attractive to compensate for the loss of information in amplitude given by the low resolution of the ADC by oversampling. In this sense, the advantages of oversampling and time resolution have been studied in terms of the maximum achievable rate. In [3] the maximum achievable rate of a Zakai bandlimited process that carries information through the signs of the signal was studied and it is shown that it improves considerably with oversampling. The main idea of the study in [3] is to show that a bandlimited process exist that has zero-crossings at the desired time instances. This was shown by a process which does not have a Fourier representation but the process is bandlimited according to Zakai's bandlimitation criterion.

Other investigations in terms of capacity that show the benefits of oversampling are presented in [4] and [5]. In [5] the maximum achievable rate is studied for a bandlimited channel with additive white Gaussian noise where the results showed considerable gain when using oversampling.

Studies concerning to communication systems with 1-bit quantization and oversampling at the receiver are carried out in [6], where the filter coefficients are optimized for the waveform design in terms of a maximization of the minimum distance to the decision threshold at the receiver. The previous criterion was established in [7, 8, 9] for other channels with hard detection. Other studies based on the maximization of the minimum distance to the decision threshold (MMDDT) approach presented in [6] were done in [10] where the criterion was adopted for a multiple-input single-output (MISO) system.

With the exponential growth of the number of users and the amount of information, this new use of IoT communication networks brings a lot of challenges related to high capacities, high data rates, massive devices connections and cost reduction. In order to serve millions of devices and to fulfill the future connections requirements in the same network, Multi-Input Multiple Output (MIMO) systems with low resolution in the ADC are promising for IoT networks. In this sense the study from [6] is extended to a massive MIMO system with a bandlimited channel in the work done in [11] where besides performing the MMDDT criterion the approach in [11] relies on a dynamic optimization which involves a forward mapping strategy.

1.2 Contributions

The scope of this work lies in the design of precoding techniques for receivers with one bit quantization and oversampling and the precoding design shall enable the use of low-complexity receivers. In this context it is aimed to develop new methods which outperform the most promising state-of-the-art methods in terms of bit error rate and computational complexity.

The main contribution of this work is the zero-crossing modulation, where the information is conveyed within the time instances of zero-crossing, similar as it was presented in [3] and different to the forward mapping strategy presented in [11]. The zero-crossing modulation was implemented with two precoders, the temporal MMDDT precoder together with the spatial zero forcing (ZF) precoding and the space-time minimum mean square error (MMSE) precoding. Numerical results confirm that the MMSE precoding design presents better performance for low signal-to-noise values as compared to the MMDDT which has better results in cases of high signal-to-noise values.

The simulation results showed significantly the advantages of zero-crossing modulation over the state-of-the-art method [11] and opens the possibility for future works based on zero-crossing modulation that contribute to the development of new communication technologies.

1.3
Structure of the work

The ensuing work consists of 7 chapters which are structured as follows:

In Chapter 2 the state-of-the-art is developed, where the previous studies that motivated the realization of this work are detailed. In addition the method of quantization precoding [11] is carefully described, as it is the method against which this work is compared.

The Chapter 3 introduces a single-input single-output (SISO) system that allows the description of the main elements of the system. Also, a discrete system model is presented. This chapter also describes the novel zero-crossing modulation process that is the main contribution of this work and explains how the information is conveyed in the zero-crossing time instances of the received signal. In addition, a bit mapping scheme based on Gray coding is introduced.

Chapter 4 presents the extension of the Chapter 3 to a multiuser MIMO system with 1-bit quantization and oversampling. This chapter describes the channel and mainly the two precoding techniques: the temporal MMDDT precoder and the space-time MMSE precoder, both with zero-crossing modulation. The chapter ends with simulation results for different oversampling factors which are compared with the state-of-the-art with the forward mapping (FM) approach from [11]. The influence of the bandwidth on the maximum distance to the decision threshold (γ) and on the mean square error (MSE) are also shown.

The analysis of the interblock interference effect over the precoders is analyzed in Chapter 5. Chapter 6 makes an analysis of the FM and zero-crossing approaches with the performance comparison in terms of bit error rate (BER).

The final Chapter 7 concludes the work highlighting the most important results and the research topics that can be addressed in the future.

1.4 Notation

To ensure readability and consistency in the document, the notation presented in Table 1.1 is introduced to be used throughout the document. As a clarification, the tilde symbol on the top is used to represent complex quantities or complex values while the lack of this implies only the real part of a complex value.

Table 1.1: Notation summary

Declaration	Notation	Example
Complex value	$\tilde{x}$	$\tilde{x}_i$
Real value	x	γ
Complex vector	$\tilde{\boldsymbol{x}}$	$\tilde{\boldsymbol{p}}_{\mathrm{x}}$
Matrix	$\boldsymbol{X}$	$\boldsymbol{G}_{\mathrm{Rx}}$
Complex matrix	$\tilde{\boldsymbol{X}}$	$\tilde{\boldsymbol{H}}$

2
State-of-the-art

In recent years the development of new communication technologies, such as multigigabit per second communications which include millimeter wave communications [12] or high-impact applications as IoT that require low complexity devices in the terminals, a bottleneck has been found with the ADC due to the high energy consumption and its high complexity because of its high resolution in amplitude.

The idea of using 1-bit receivers combined with oversampling aims to be the solution for this bottleneck problem with the ADC, being the oversampling the way to compensate the loss of information in amplitude by moving that information to the temporal dimension (see Fig. 2.1).

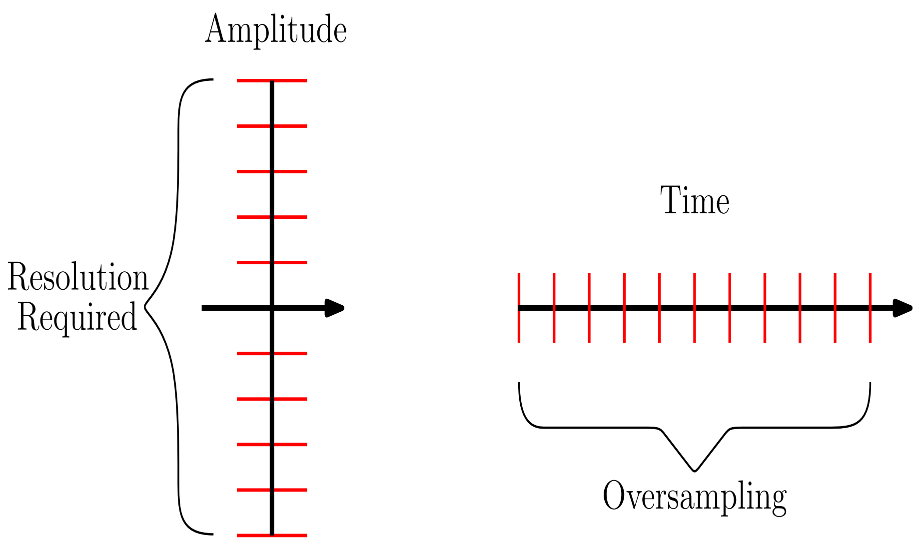

Figure 2.1: Time vs amplitude procesing

In this sense, Shamai in [3] studied the maximum achievable rate carried by the sign of a Zakai bandlimited process sampled n times at the Nyquist rate.

Studies conducted based on oversampling have shown promising results despite the significant restrictions regarding the possibility of engineering communications systems with 1-bit receivers. The use of low resolution devices has opened the way for the study of new processing techniques such as zero-crossing modulation. In this sense, Shamai in [3] studied the maximum achievable rate carried by the sign of a Zakai bandlimited process sampled with n times the Nyquist rate. Shamai shows that a Zakai bandlimited process [13] can be constructed with one zero-crossing per Nyquist interval and with L zero-crossings per each L-Nyquist interval reaching an achievable rate of $f = \log_2(n+1)$ bits per Nyquist interval. Moreover it was also demonstrated that the information rate carried in the signs increases with the oversampling factor.

Other works such as Landau et al. [14] exploit the approach of faster-than-Nyquist (FTN) signaling for sequence design optimization using 1-bit quantization and oversampling at the receiver. The design strategies, unlike the works mentioned above, consist of the use of run-length limited sequences and the optimization of the Markov source, showing favorable results in terms of achievable rate compared to methods with conventional signaling rates factors.

Spectral efficient modulation schemes where investigated by Landau et al. in [6] for receivers with 1-bit quantization and oversampling. The work proposes an inter-symbol interference (ISI) filter optimization such that the waveform design has as objective function the maximization of the maximum distance to the decision threshold for samples at the receiver, prior to quantization as it is shown in Fig. 2.2

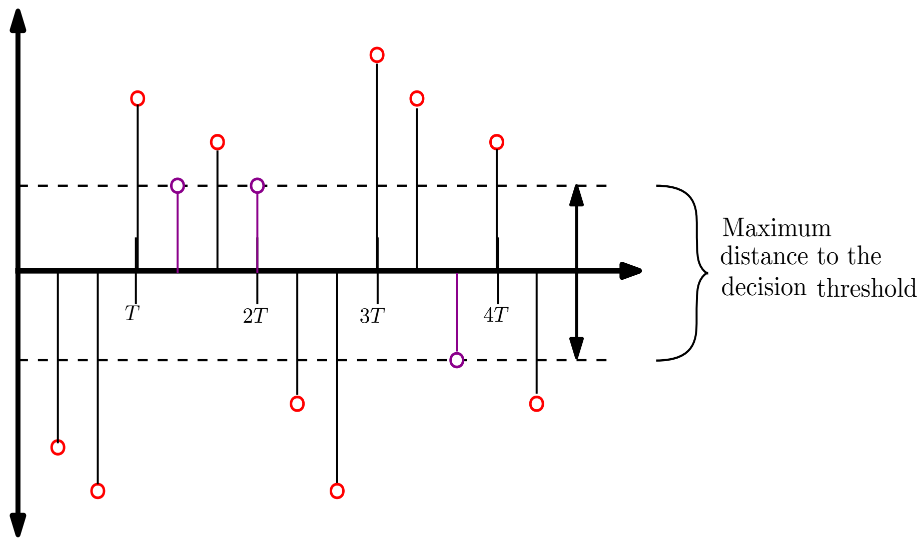

Figure 2.2: Maximum distance to the decision threshold example

Other studies based on work done in [6] as [10] also exploit the oversampling property to optimize the waveform design through the maximization of the minimum distance to the decision threshold for a massive MISO narrowband downlink system. The waveform design optimization is aimed at the development of algorithms that efficiently design the filter coefficients. In addition, the work presents a simple detector approach with the use of Hamming distance.

The most recent study, focused on 1-bit waveform design optimization with oversampling at the receiver is done in [11] for a multiuser massive MIMO downlink system with band limitation. This paper presents a two-stage precoding approach: the temporal one called quantization precoding and the spatial channel precoder with ZF.

The output of the quantization precodign is formulated as the solution of a constrained convex optimization problem. The restrictions are given by the total transmitted energy, the amount of out-of-band radiation allowed and the bandwidth limitation given by the transmit and receive filters.

Initially, the different possible quantized outputs or codewords, used to perform the symbol-to-symbol mapping called forward mapping, are generated. The number of codebooks or FMs is determined by the oversampling factor and the modulation order per real dimension. For an order of cardinality $R_{\text{in}} = 4$ and an oversampling factor of $M_{\text{Rx}} = 2$, there are 24 different FMs and for an oversampling factor of 3 there are 1680 FMs. The number of the different possibles FMs is given by

$$\text{total}_{\text{FMs}} = \binom{R_{\text{in}}}{R_{\text{out}}} R_{\text{in}}!, \tag{2-1}$$

where $R_{\text{out}} = 2^{M_{\text{Rx}}}$.

The convex optimization problem that aims to maximize the minimum distance to the decision threshold is solved for each of the FMs in order to find the FM that provides the largest minimum distance to the decision threshold.

The received signal is quantized to 1-bit and the backward mapping (BM) modulation is performed for the detection process. This BM modulation is defined as an inverse process to the FM modulation. The detection process is elaborated using the Hamming distance metric, as it was proposed in [10].

For the case of massive MIMO with a large number of transmit antennas, the spatial precoder provides a high beamforming gain that increases with the number of transmitting antennas.

3
SISO system model

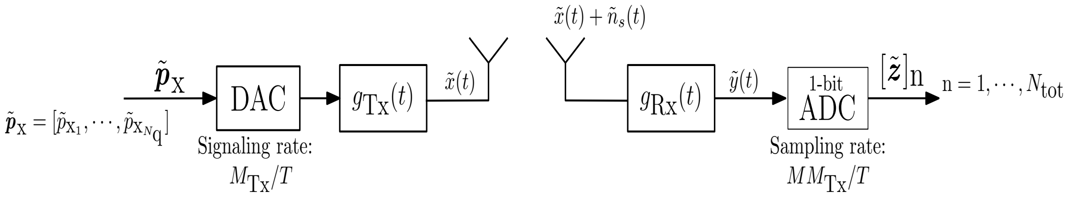

Figure 3.1: SISO system model

Initially a SISO system model is considered to introduce the basic elements that compose it and also to describe the discrete system model. These elements remain the same in the extensions to multiuser MIMO that are presented later in Chapter 4.

The SISO system model is considered as illustrated in Fig. 3.1. where the transmitter, the channel and the receiver are the main components that integrate it. In this chapter all this components are detailed and later the equivalent discrete system model is presented.

3.1
Transmitter

The input block sequence $\tilde{\boldsymbol{x}}$, of N complex symbols each one denoted as $\tilde{x}_i = x_i^I + x_i^Q$ and emitted with symbol duration T, is mapped into the vector $\tilde{\boldsymbol{p}}_{\mathrm{x}}$ through the space and time precoders that will be detailed more deeply in Chapter 4. Each symbol x_i from the sequence $\tilde{\boldsymbol{x}}$ is drawn from the set $\mathcal{X}_{\mathrm{in}}$ whose cardinality is given by $R_{\mathrm{in}} = M_{\mathrm{Rx}} + 1$. That means that the set $\mathcal{X}_{\mathrm{in}}$ is determined by the chosen of the oversampling factor M_{Rx}.

The vector $\tilde{\boldsymbol{p}}_{\mathrm{x}}$ which has dimension N_{q}, where $N_{\mathrm{q}} = M_{\mathrm{Tx}}N + 1$ is converted to a continuous waveform through the digital-to-analog converter (DAC) and the pulse shaping filter with impulse response $g_{\mathrm{Tx}}(t)$. The DAC is assumed to be perfect such that $\sum_{i=-\infty}^{\infty} \tilde{x}_i \delta\left(t - i\frac{T}{M_{\mathrm{Tx}}}\right)$.

$\frac{M_{\mathrm{Tx}}}{T}$ describes the signaling rate and is utilized for increasing the spectral efficiency where the signaling factor $M_{\mathrm{Tx}} > 1$ correspond to the FTN signaling approach introduced in [15].

The pulse shaping filter g_{Tx} is a raised-cosine (RC) filter with roll-off factor ϵ_{Tx} and bandwidth determined by $W_{\mathrm{Tx}} = (1+\epsilon_{\mathrm{Tx}})/T_{\mathrm{s}}$ whose impulse response is given by

$$g_{\mathrm{Tx}}(t) = \begin{cases} \frac{\pi}{4T_s}\mathrm{sinc}\left(\frac{1}{\epsilon_{\mathrm{Tx}}}\right), & t = \pm\frac{T_s}{2\epsilon_{\mathrm{Tx}}} \\ \frac{1}{T_s}\mathrm{sinc}\left(\frac{t}{T_s}\right)\frac{\cos\left(\frac{\pi\epsilon_{\mathrm{Tx}}t}{T_s}\right)}{1-\left(\frac{2\epsilon_{\mathrm{Tx}}t}{T_s}\right)}, & \text{otherwise} \end{cases} \tag{3-1}$$

and is illustrated in Fig. 3.2. The pulse duration T_{s} is not always the same as T as in the cases in which the influence of the bandwith over the MDDT and the MSE is studied.

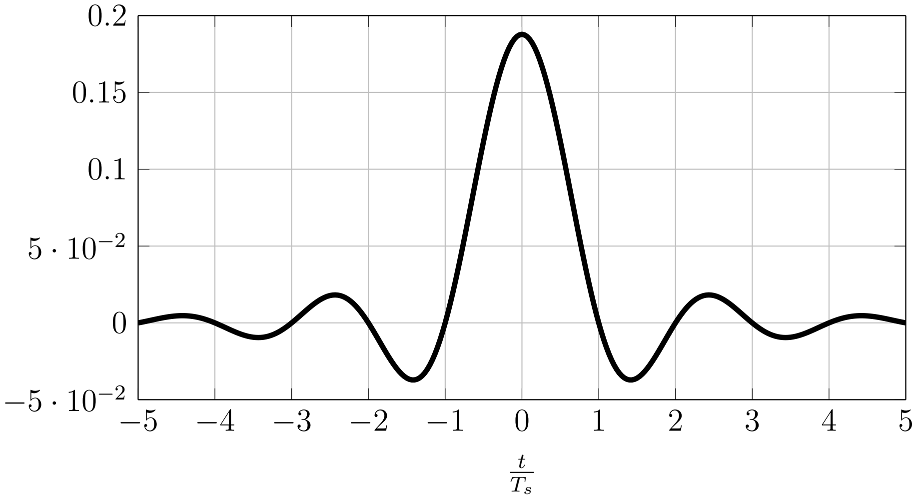

Figure 3.2: Impulse response of the RC filter with roll-off factor $\epsilon_{\mathrm{Tx}} = 0.22$

In the study, it is considered that the transmit filter is normalized to unit energy such that

$$\int_{-\infty}^{\infty} |g_{\mathrm{Tx}}(t)|^2\, dt = 1. \tag{3-2}$$

3.2 Channel

The channel is considered an AWGN. The noise $\tilde{n}(t)$ is complex Gaussian distributed with zero mean and variance $\sigma_{\tilde{n}}^2$.

3.3 Receiver

The receiver consists mainly of two components, the pulse shaping filter $g_{\mathrm{Rx}}(t)$ and the analog-to-digital converter (ADC). The $g_{\mathrm{Rx}}(t)$ filter is a square-root raise cosine filter (RRC) with roll-off factor ϵ_{Rx} and bandwidth

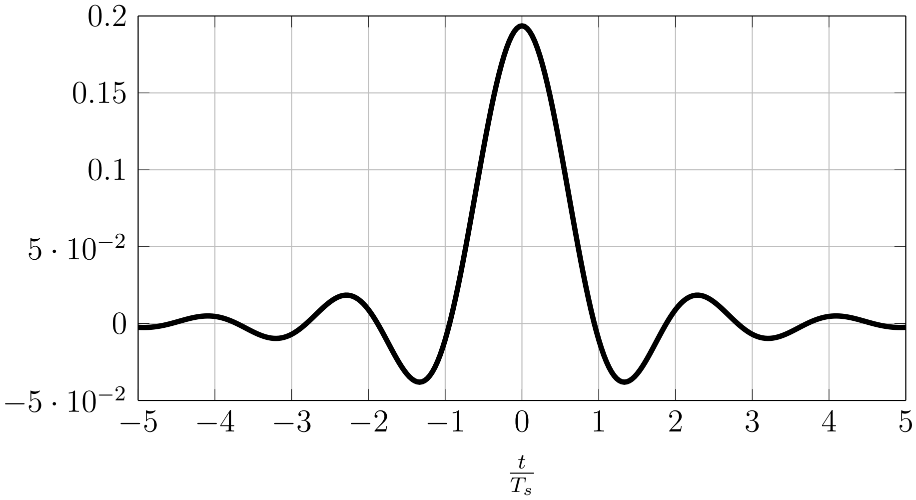

Figure 3.3: Impulse response of the RRC filter with roll-off factor $\epsilon_{\mathrm{Tx}} = 0.22$

$W_{\mathrm{Rx}} = W_{\mathrm{Tx}} = (1 + \epsilon_{\mathrm{Tx}})/T_{\mathrm{s}}$. The graphic representation is shown in Fig. 3.3 and the impulse response is given by

$$g_{\mathrm{Rx}}(t) = \begin{cases} \frac{1}{T_s}\left(1 + \beta\left(\frac{4}{\pi} - 1\right)\right), & t = 0 \\ \frac{\beta}{T_s\sqrt{2}}\left[\left(1 + \frac{2}{\pi}\right)\sin\left(\frac{\pi}{4\beta}\right) + \left(1 - \frac{2}{\pi}\right)\cos\left(\frac{\pi}{4\beta}\right)\right], & t = \pm\frac{T_s}{4\beta} \\ \frac{1}{T_s}\frac{\sin\left[\pi\frac{t}{T_s}(1-\beta)\right] + 4\beta\frac{t}{T_s}\cos\left[\pi\frac{t}{T_s}(1+\beta)\right]}{\pi\frac{t}{T_s}\left[1 - \left(4\beta\frac{t}{T_s}\right)^2\right]}, & \text{otherwise} \end{cases} \tag{3-3}$$

In this study, it is considered that also the receive filter has unit energy such that

$$\int_{-\infty}^{\infty} |g_{\mathrm{Rx}}(t)|^2 \, dt = 1. \tag{3-4}$$

The combined waveform determined by the transmit and receive filter can be described by the convolution $v(t) = g_{\mathrm{Tx}}(t) * g_{\mathrm{Rx}}(t)$. The received signal is processed by the $g_{\mathrm{Rx}}(t)$ filter and the input signal to the ADC is given by:

$$y(t) = \int_{-\infty}^{\infty}\left(\sum_{i=-\infty}^{\infty} \tilde{x}_i \delta(t - iT) * g_{\mathrm{Tx}} + n(t)\right) * g_{\mathrm{Rx}}. \tag{3-5}$$

At the ADC the signal $\tilde{y}(t)$ is oversampled at a rate $\frac{M_{\mathrm{Rx}}}{T} = \frac{MM_{\mathrm{Tx}}}{T}$, where $M_{\mathrm{Tx}} > 1$ corresponds to faster-than-Nyquist signaling and $M_{\mathrm{Rx}} = 1$ means no oversampling. Given the oversampling factor M_{Rx} and the length of the transmitted block the length of the sampled signal $\tilde{\boldsymbol{y}}$ is N_{tot}, where $N_{\mathrm{tot}} = M_{\mathrm{Rx}}N + 1$. Then, the signal $\tilde{\boldsymbol{y}}$ is quantized to one bit according to

$$\tilde{\boldsymbol{z}} = Q1(\tilde{\boldsymbol{y}}) = \mathrm{sign}(\mathrm{Real}\{\tilde{\boldsymbol{y}}\}) + j\mathrm{sign}(\mathrm{Imag}\{\tilde{\boldsymbol{y}}\}). \tag{3-6}$$

The quantization process is assumed to be independent for the real and imaginary parts of $\tilde{x}_i$, therefore two quantizers are assumed.

3.4 Discrete system model

To be able to simulate the proposed system it is necessary to go from continuous time to discrete time. In discrete representation, the filters $g_{\mathrm{Tx}}(t)$ and $g_{\mathrm{Rx}}(t)$ become the vectors $\boldsymbol{g}_{\mathrm{Tx}}$ and $\boldsymbol{g}_{\mathrm{Rx}}$ respectively, which contain the coefficients for different instants of time of $g_{\mathrm{Tx}}(t)$ and $g_{\mathrm{Rx}}(t)$. The discrete quantized receive signal is denoted as

$$\tilde{\boldsymbol{z}} = Q_1\left(\tilde{\boldsymbol{y}}\right) = Q_1\left(\boldsymbol{V}\boldsymbol{U}\tilde{\boldsymbol{p}}_x + \boldsymbol{G}_{\mathrm{Rx}}\tilde{\boldsymbol{n}}\right), \tag{3-7}$$

where $\tilde{\boldsymbol{n}}$ is the vector that contains the complex Gaussian noise samples with zero mean and variance $\sigma_{\tilde{n}}^2$. $\boldsymbol{U}$ is the M-fold upsampling matrix with dimensions $N_{\mathrm{tot}} \times N_{\mathrm{q}}$ which is defined as

$$\boldsymbol{U}_{m,n} = \begin{cases} 1, & \text{for} \quad m = M \cdot (n-1) + 1 \\ 0, & \text{else,} \end{cases} \tag{3-8}$$

where, m and n are positive integers that symbolize the row and column index, respectively. $\boldsymbol{V}$ is a Toeplitz matrix containing the coefficients of the waveform impulse response $v(t)$ with size $N_{\mathrm{tot}} \times N_{\mathrm{tot}}$ denoted as

$$\boldsymbol{V} = \begin{bmatrix} v\left(0\right) & v\left(\frac{T}{M_{\mathrm{Rx}}}\right) & \cdots & v\left(TN\right) \\ v\left(-\frac{T}{M_{\mathrm{Rx}}}\right) & v\left(0\right) & \cdots & v\left(T\left(N - \frac{1}{M_{\mathrm{Rx}}}\right)\right) \\ \vdots & \vdots & \ddots & \vdots \\ v\left(-TN\right) & v\left(T\left(-N + \frac{1}{M_{\mathrm{Rx}}}\right)\right) & \cdots & v\left(0\right) \end{bmatrix}. \tag{3-9}$$

The $\boldsymbol{G}_{\mathrm{Rx}}$ Toeplitz matrix represents the receiver filter g_{Rx} and is structured as follows

$$\boldsymbol{G}_{\mathrm{Rx}} = a_{\mathrm{Rx}} \begin{bmatrix} \left[\ \boldsymbol{g}_{\mathrm{Rx}}^T\ \right] & 0 \cdots & 0 \\ 0 & \left[\ \boldsymbol{g}_{\mathrm{Rx}}^T\ \right] & 0 \cdots 0 \\ & \ddots\ \ddots\ \ddots & \\ 0 \cdots & 0 & \left[\ \boldsymbol{g}_{\mathrm{Rx}}^T\ \right] \end{bmatrix}_{N_{\mathrm{tot}} \times 3N_{\mathrm{tot}}}, \tag{3-10}$$

with $\boldsymbol{g}_{\mathrm{Rx}} = [g_{\mathrm{Rx}}(-T(N+\frac{1}{M_{\mathrm{Rx}}})), g_{\mathrm{Rx}}(-T(N+\frac{1}{M_{\mathrm{Rx}}})+\frac{T}{M_{\mathrm{Rx}}}), \ldots, g_{\mathrm{Rx}}(T(N+\frac{1}{M_{\mathrm{Rx}}}))]^T$ as the coefficients of the $g_{\mathrm{Rx}}(t)$ filter and $a_{\mathrm{Rx}} = (T/M_{\mathrm{Rx}})^{1/2}$ as the normalization factor that in continuous time is represented by the normalization to unit energy . The corresponding Toeplitz matrix that contains the coefficients of the transmit filter g_{Tx} is defined as

$$\boldsymbol{G}_{\mathrm{Tx}} = a_{\mathrm{Tx}} \begin{bmatrix} \left[\ \boldsymbol{g}_{\mathrm{Tx}}^{T}\ \right] & 0\cdots & 0 \\ 0 & \left[\ \boldsymbol{g}_{\mathrm{Tx}}^{T}\ \right] & 0\cdots 0 \\ & \ddots\ \ddots\ \ddots & \\ 0\cdots & 0 & \left[\ \boldsymbol{g}_{\mathrm{Tx}}^{T}\ \right] \end{bmatrix}_{N_{\mathrm{tot}}\times 3N_{\mathrm{tot}}}, \tag{3-11}$$

with $\boldsymbol{g}_{\mathrm{Tx}} = [g_{\mathrm{Tx}}(-T(N+\frac{1}{M_{\mathrm{Rx}}})), g_{\mathrm{Tx}}(-T(N+\frac{1}{M_{\mathrm{Rx}}})+\frac{T}{M_{\mathrm{Rx}}}), \ldots, g_{\mathrm{Tx}}(T(N+\frac{1}{M_{\mathrm{Rx}}}))]^{T}$ and normalization factor $a_{\mathrm{Tx}} = (T/M_{\mathrm{Rx}})^{1/2}$. The factors a_{Tx} and a_{Rx} represent the normalization that in continuous time are given by (3-2) and (3-4), respectively.

3.5
Zero-crossing modulation

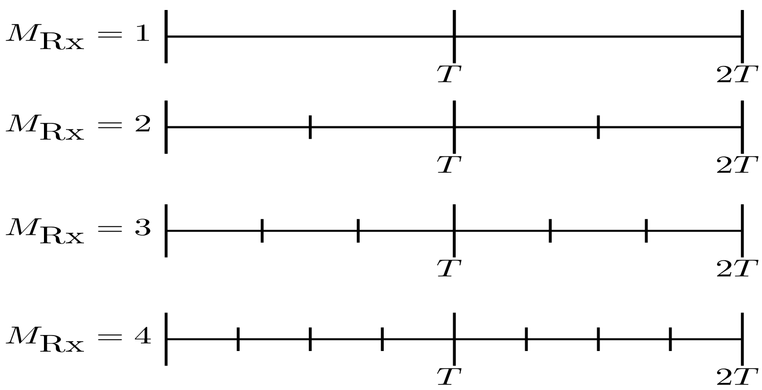

Figure 3.4: Sampling instances for $M_{\mathrm{Rx}} = 1, 2, 3, 4$

In [3] is studied the construction of a bandlimited signal by their sign information. The study starts from the construction of a bounded Zakai process [13] and it is extended to a process with L zero-crossings per each L-Nyquist interval. In terms of the achievable rate, the study shows that for a Zakai bandlimited process the information rate carried in the signs increases with the oversampling factor. Based on the above we have performed a mapping process which conveys the information in the zero-crossing time instances of the received signal.

Unlike the method in [3], the proposed method includes also the non-zero-crossing per time interval transmit symbol (absence of zero-crossing), which implies a relief of the waveform design when considering the same cardinality of input alphabet. In other words, for the novel precoding method we allocate at max one zero-crossing per symbol interval. It means that all the symbols x_i, taken from the set $\mathcal{X}_{\text{in}} = \{b_1, b_2 \cdots, b_{R_{\text{in}}}\}$, are mapped into a codeword defined by the time instant, within the symbol interval, in which the zero-crossing occurs or not.

To make way for the design of the corresponding transmit vector $\boldsymbol{p}_{\text{x}}$ we start with the forward mapping process with the construction of a binary sequence denoted as $\boldsymbol{c}_{\text{out}}$ which is desired at the receiver after the quantization.

Given an oversampling factor, each Nyquist interval is divided in M_{Rx} segments as is shown in Fig. 3.4. The main idea of the proposed zero-crossing modulation is that each symbol b_j, is defined according to presence or not of a zero-crossing in an specific segment inside of the Nyquist interval. For this, it is established a mapping table $\boldsymbol{c}_{\text{map}}$ which relates each symbol b_j with the time instance within the Nyquist interval where the zero-crossing occurs. In the Table 3.1 the zero-crossing assignment is presented for $M_{\text{Rx}} = 3$.

Table 3.1: $\boldsymbol{c}_{\text{map}}$ for $M_{\text{Rx}} = 3$

$\boldsymbol{c}_{\text{map}}$	
symbol	Zero-crossing assignment
b_1	Non zero-crossing
b_2	Zero-crossing in the third interval
b_3	Zero-crossing in the second interval
b_4	Zero-crossing in the first interval

According with the last, a fixed mapping is considered and it is assumed to be known at the receivers, which is a benefit in comparison to the approach in [11], where the dynamic mapping tables require additional bandwidth for informing the receivers.

Once the table mapping $\boldsymbol{c}_{\text{map}}$ is established, each symbol x_i taken from the input sequence $\boldsymbol{x}$ is mapped in a codeword $\boldsymbol{c}_s$ of length M_{Rx} which specifies in which Nyquist interval the zero-crossing occurs or not.

Since the coding depends on the time instant of the zero-crossing and therefore in $\boldsymbol{c}_{\text{map}}$ the codeword construction is based on the last sample, denominated ρ, of the previous symbol interval $\boldsymbol{c}_{s_{i-1}}$. This means that each symbol b_j can be mapped in two codewords as can be observed in Fig. 3.5 where each symbol meets the requirements of $\boldsymbol{c}_{\text{map}}$ in two different ways: one for $\rho = 1$ and another for $\rho = -1$. In the Fig. 3.5 the red line implies a previous sample $\rho = 1$ and the blue one a previous sample $\rho = -1$.

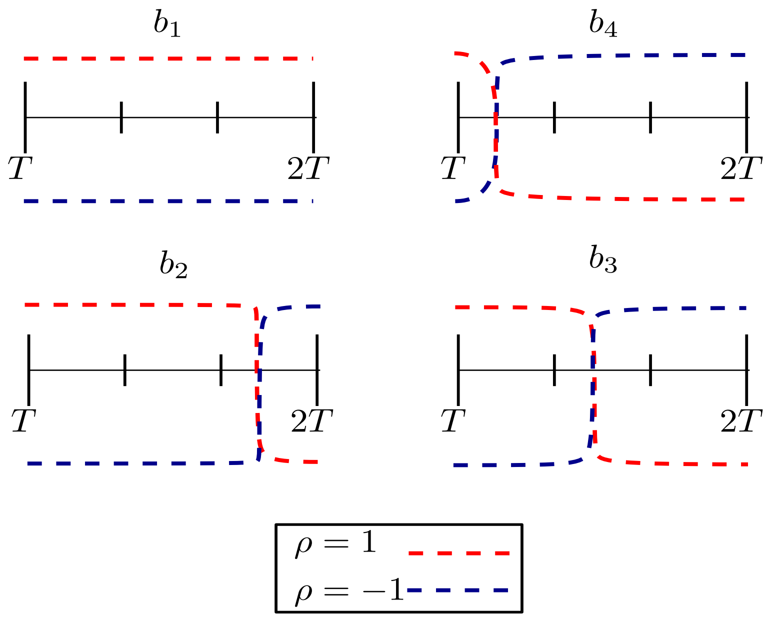

Figure 3.5: Illustration that explains the dependency of $\boldsymbol{c}_s$ on ρ according Table 3.1

The last means that the $\boldsymbol{c}_s$ segment is constructed depending on whether ρ is 1 or -1, meaning that each symbol b_j can be mapped in two code segments fulfilling the $\boldsymbol{c}_{\text{map}}$ assignments. In terms of samples in Table 3.2 and Table 3.3 it is shown the structure of $\boldsymbol{c}_s$ according to ρ for $M_{\text{Rx}} = 2$ and $M_{\text{Rx}} = 3$ respectively.

Table 3.2: $\boldsymbol{c}_{\text{s}}$ for $M_{\text{Rx}} = 2$

	$\boldsymbol{c}_s$	
Symbol	$\rho_{i-1} = 1$	$\rho_{i-1} = -1$
b_1	$1 \quad 1$	$-1 \quad -1$
b_2	$1 \quad -1$	$-1 \quad 1$
b_3	$-1 \quad -1$	$1 \quad 1$

Given the dependency of $\boldsymbol{c}_{\text{s}}$ in the last sample of $\boldsymbol{c}_{\text{s},i-1}$, to enable the mapping process of the first symbol of $\tilde{\boldsymbol{x}}$, a pilot signal $pb \in 1, -1$ is included as the first sample of $\boldsymbol{c}_{\text{out}}$ to initiate the processes. In other words pb plays the role of ρ to map the symbol $\tilde{x_1}$.

Finally, the desired binary output pattern $\boldsymbol{c}_{\text{out}}$ for a sequence of N symbols, which yields the zero-crossings in the desired intervals is constructed sequentially by concatenation of sequence segments $\boldsymbol{c}_{\text{s},i}$. At the end the size of $\boldsymbol{c}_{\text{out}}$ results in a vector of length $NM_{\text{Rx}} + 1$.

It is of great importance to highlight that the mapping process described above is realized independently and identically for the real and imaginary parts

Table 3.3: $\boldsymbol{c}_\mathrm{s}$ for $M_\mathrm{Rx} = 3$

	$\boldsymbol{c}_s$	
Symbol	$\rho_{i-1} = 1$	$\rho_{i-1} = -1$
b_1	$1 \quad 1 \quad 1$	$-1 \ -1 \ -1$
b_2	$1 \quad 1 \ -1$	$-1 \ -1 \quad 1$
b_3	$1 \ -1 \ -1$	$-1 \quad 1 \quad 1$
b_4	$-1 \ -1 \ -1$	$1 \quad 1 \quad 1$

of each symbol $\tilde{x}_i$.

Lets take as an example the input sequence $\tilde{\boldsymbol{x}} = [b_1, b_3, b_2, b_0, b_2, b_1]$ with $N = 6$, $M_\mathrm{Rx} = 3$ and the random pilot signal $pb = 1$. So, the mapping sequence of length 19 constructed as $\boldsymbol{c}_\mathrm{out} = [pb, \boldsymbol{c}_{\mathrm{s},1}, \cdots, \boldsymbol{c}_{\mathrm{s},i}, \cdots, \boldsymbol{c}_{\mathrm{s},N}]$ for the real part of $\tilde{\boldsymbol{x}}$ will be:

$$\boldsymbol{c}_\mathrm{out} = [1\ 1\ 1\ 1\ -1\ 1\ 1\ 1\ 1\ -1\ -1\ -1\ -1\ -1\ -1\ 1\ 1\ 1\ 1\ 1]$$

The graphic representation of the last example is illustrated in Fig. 3.6 where it can be seen more clearly the action of ρ and pb. Moreover it is observed how the symbol b_2 can be represented by two different sequences of samples $\boldsymbol{c}_{\mathrm{s},3} = [1 - 1 - 1]$ and $\boldsymbol{c}_{\mathrm{s},5} = [-111]$ since $\rho_2 = 1$ and $\rho_4 = -1$ even so it still meets the $\boldsymbol{c}_\mathrm{map}$ assignment of having a zero-crossing in the second interval.

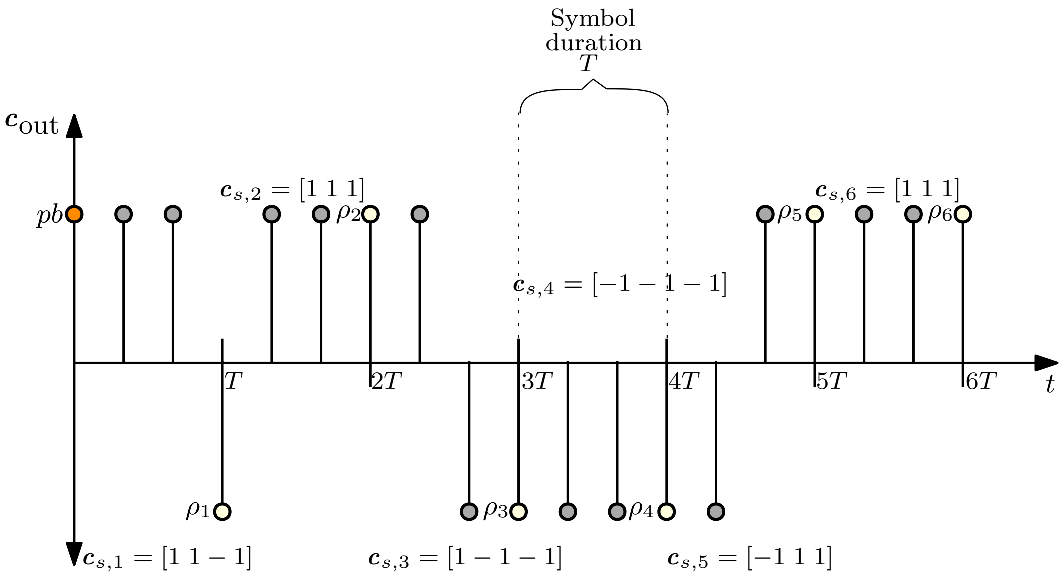

Figure 3.6: Example of the construction of $\boldsymbol{c}_\mathrm{out}$ for $M_\mathrm{Rx} = 3$

The following section describes the process that was carried out to devise a bit-mapping scheme for the zero-crossing modulation similar to Gray-coding once a random input sequence of bits is given.

3.6 Gray coding for zero-crossing precoding

The Gray coding is a binary coding system designed to facilitate error correction. The Gray encoding function is to minimize the number of errors in the process of going from symbols to bits ensuring that adjacent symbols differ in one bit only. Fig. 3.7 illustrates the Gray coding for quadrature phase shift keying (QPSK) symbols.

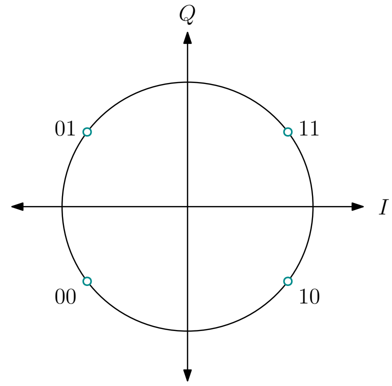

Figure 3.7: Gray coding for QPSK symbols

For zero-crossing modulation, given a random transmitted bit sequence, the design of a *Gray* code is proposed to improve the system performance in terms of BER. The main idea of the *Gray* code is that symbols that have near or consecutive zero-crossings differ only in one bit from another.

Since the cardinality of the symbol alphabet depends on R_{in}, we have established the basis to go from bits to symbols in terms of θ and λ which correspond to positive integers where θ determines the number of bits and λ the number of symbol tuples or symbols set so that it is fulfilled (3-12). Then it is possible to construct a symbol sequence that complies with the following condition:

$$2^{\theta} \leq R_{\mathrm{in}}^{\lambda} \tag{3-12}$$

For the case of $M_{\mathrm{Rx}} = 3$, we have $R_{\mathrm{in}} = 4$ hence equality holds when 2 bits can be mapped to one symbol, this is $\lambda = 1$ and $\theta = 2$ which means that there is no loss of information. In the Table 3.4 it is shown the gray mapping for $M_{\mathrm{Rx}} = 3$ where each binary tuple is mapped in just one symbol, then the sequence $\boldsymbol{c}_{\mathrm{s}}$ is presented for each symbol according to ρ.

Table 3.4: *Gray code* for $M_{\mathrm{Rx}} = 3$

$M_{\mathrm{Rx}} = 3$		
Gray code	$\boldsymbol{c}_{\mathrm{s}}\ (\rho_{i-1} = 1)$	$\boldsymbol{c}_{\mathrm{s}}\ (\rho_{i-1} = -1)$
00	$1 \quad 1 \quad 1$	$-1 \ -1 \ -1$
01	$1 \quad 1 \ -1$	$-1 \ -1 \quad 1$
11	$1 \ -1 \ -1$	$-1 \quad 1 \quad 1$
10	$-1 \ -1 \ -1$	$1 \quad 1 \quad 1$

For the case of $M_{\mathrm{Rx}} = 2$ it is not possible to reach the equality of (3-12), as in the case with $M_{\mathrm{Rx}} = 3$, thus values for λ and θ are considered so that the loss of information due to the conversion process is minimized. Accordingly, sets or subsequences of symbols are considered taking $\lambda = 2$ and $\theta = 3$.

Given that $(2^{\theta} = 8) < (R_{\mathrm{in}}^{\lambda} = 9)$, that is the number of bit tuples is smaller than the number of subsequences of $\lambda = 2$ symbols that can be formed, one subsequence of symbols is excluded in the mapping process.

Considering a set $\mathcal{X}_{\mathrm{in}} = \{b_1, b_2, b_3\}$ the 9 subsequences that can be made up with $\lambda = 2$ are presented in Table 3.5.

Table 3.5: Symbol combination for $M_{\mathrm{Rx}} = 2$

$M_{\mathrm{Rx}} = 2$		
Symbol set	$[\boldsymbol{c}_{\mathrm{s},2i}^T, \boldsymbol{c}_{\mathrm{s},2i+1}^T]$ $\rho_{2i-1} = 1$	$[\boldsymbol{c}_{\mathrm{s},2i}^T, \boldsymbol{c}_{\mathrm{s},2i+1}^T]$ $\rho_{2i-1} = -1$
b_1b_1	$1 \quad 1 \quad 1 \quad 1$	$-1 \ -1 \ -1 \ -1$
b_1b_2	$1 \quad 1 \quad 1 \ -1$	$-1 \ -1 \ -1 \quad 1$
b_1b_3	$1 \quad 1 \ -1 \ -1$	$-1 \ -1 \quad 1 \quad 1$
b_2b_1	$1 \ -1 \ -1 \ -1$	$-1 \quad 1 \quad 1 \quad 1$
b_2b_2	$1 \ -1 \ -1 \quad 1$	$-1 \quad 1 \quad 1 \ -1$
b_2b_3	$1 \ -1 \quad 1 \quad 1$	$-1 \quad 1 \ -1 \ -1$
b_3b_1	$-1 \ -1 \ -1 \quad 1$	$1 \quad 1 \quad 1 \ -1$
b_3b_2	$-1 \ -1 \ -1 \ -1$	$1 \quad 1 \quad 1 \quad 1$
b_3b_3	$-1 \ -1 \quad 1 \quad 1$	$1 \quad 1 \ -1 \ -1$

In this special case, to select the subsequence of symbols it was taken as criteria the closeness of zero-crossings as it supposes greatest difficulty for the waveform design optimization. Then, the symbol subsequence where two zero-crossing time instances are close to each other was excluded from the set. The subsequence that presents the closest zero crossings is that given by b_2b_3 as it is shown in Fig. 4.3.

Finally the the proposed *Gray* code developed for $M_{\mathrm{Rx}} = 2$ is shown in the Table 3.6 where the subsequence $[1 \ -1 \quad 1 \quad 1]$ was excluded which

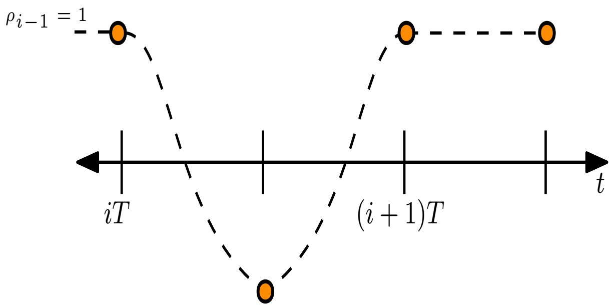

Figure 3.8: Representation of the subsequence $b_2 b_3$

implies a conversion loss of $(1.5 - \log_2 3) \approx 0.085$ bits per symbol which does not represent a considerable loss.

Table 3.6: Proposed *Gray code* for $M_{\text{Rx}} = 2$

$M_{\text{Rx}} = 2$		
Gray Code	$[\boldsymbol{c}^T_{\text{s},2i}, \boldsymbol{c}^T_{\text{s},2i+1}]$ $\rho_{2i-1} = 1$	$[\boldsymbol{c}^T_{\text{s},2i}, \boldsymbol{c}^T_{\text{s},2i+1}]$ $\rho_{2i-1} = -1$
000	$1 \quad 1 \quad 1 \quad 1$	$-1 \quad -1 \quad -1 \quad -1$
001	$1 \quad 1 \quad 1 \quad -1$	$-1 \quad -1 \quad -1 \quad 1$
011	$1 \quad 1 \quad -1 \quad -1$	$-1 \quad -1 \quad 1 \quad 1$
010	$1 \quad -1 \quad -1 \quad -1$	$-1 \quad 1 \quad 1 \quad 1$
110	$1 \quad -1 \quad -1 \quad 1$	$-1 \quad 1 \quad 1 \quad -1$
111	$-1 \quad -1 \quad -1 \quad 1$	$1 \quad 1 \quad 1 \quad -1$
101	$-1 \quad -1 \quad -1 \quad -1$	$1 \quad 1 \quad 1 \quad 1$
100	$-1 \quad -1 \quad 1 \quad 1$	$1 \quad 1 \quad -1 \quad -1$

4
Multiuser MIMO system

In this chapter, the SISO system presented in Chapter 3 is extended to a downlink multiuser MIMO system with band limitation. For this MIMO system two types of precoders are developed, the temporal MMDDT with spatial ZF and the space-time MMSE precoder which will be explained in the following sections, but first the channel model used for both precoders is described in the following section.

4.1
Downlink channel model

For the system described in Fig. 4.2 the channel matrix $\tilde{\boldsymbol{H}}$ with dimensions $N_\mathrm{u} \times N_\mathrm{t}$ is assumed to be *frequency-flat-fading* which means that the bandwidth of the signal is smaller than the coherence bandwidth of the channel. Therefore all frequency components of the signal will experience the same magnitude of fading [16].

The elements of $\tilde{\boldsymbol{H}}$ collect the coefficients of two fading phenomena: the small-scale fading that are attributed to the multipath propagation, reflection, dispersion, diffraction and Doppler effect. On the other hand the large-scale fading also called shadow fading is due to the path loss produced by hills or large buildings.

The matrix $\tilde{\boldsymbol{H}}$ is given by the product of the small-scale fading and the large-scale fading as described in the following way

$$\tilde{\boldsymbol{H}} = \tilde{\boldsymbol{G}}\sqrt{\boldsymbol{D}_\mathrm{H}}, \tag{4-1}$$

where $\tilde{\boldsymbol{G}}$ is the $N_\mathrm{u} \times N_\mathrm{t}$ matrix of fast fading coefficients between the base station (BS) and the N_u users described by a Rayleigh probability density function. $\boldsymbol{D}_\mathrm{H}$ is a diagonal matrix which models the geometric attenuation and shadow fading described by:

$$\boldsymbol{D}_\mathrm{H} = \frac{\boldsymbol{\zeta}}{\left(\frac{d}{r_d}\right)^{\nu}}, \tag{4-2}$$

where, d corresponds to the distance between the transmitter and the receiver, r_d is the cell radius, ν is the path loss exponent and ζ is a log-normal random variable with standard deviation σ_shadow that describes the shadow fading and has a log-normal distribution with zero mean and unit variance [17].

The noise for the MIMO system is considered as in the case of the SISO system described in Chapter 3, complex Gaussian with zero mean and variance $\sigma_{\tilde{n}}^2$.

4.2 MMDDT precoding

For the development of the Zero-Crossing Precoding with MMDDT for channels with 1-Bit quantization and oversampling, the considered MIMO system is illustrated in Fig. 4.2 with N_u single antenna users and N_t transmit antennas at the BS. The random input sequence of N symbols is generated, in this case for N_u users.

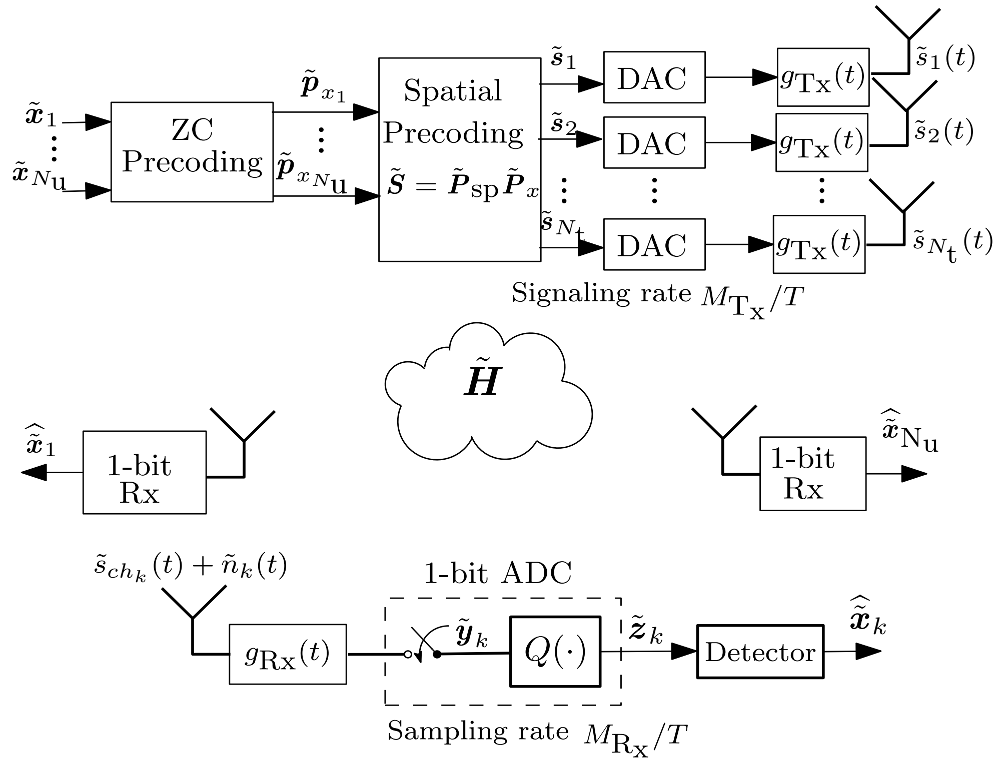

Figure 4.1: General MIMO system model

The receive signal $\tilde{\boldsymbol{Z}}$ is given by stacking the receive signal $\tilde{\boldsymbol{z}}$ of all the N_u users in the first and the N_{tot}, accounting for the different time instances, in the second dimension. The received signal can be expressed by a matrix with dimensions $N_\mathrm{u} \times N_{\mathrm{tot}}$ described by

$$\tilde{\boldsymbol{Z}} = \mathrm{Q}(\tilde{\boldsymbol{H}}\tilde{\boldsymbol{P}}_{\mathrm{sp}}\tilde{\boldsymbol{P}}_{\mathrm{x}} + \tilde{\boldsymbol{N}}\boldsymbol{G}_{\mathrm{Rx}}^T), \tag{4-3}$$

where the matrix $\tilde{\boldsymbol{N}}$ with dimensions $N_{\mathrm{u}} \times 3N_{\mathrm{tot}}$ contains i.i.d. complex Gaussian noise samples with zero mean and variance $\sigma^2_{\tilde{n}}$. The matrix $\boldsymbol{G}_{\mathrm{Rx}}$ is given by (3-10) and the matrices $\tilde{\boldsymbol{H}}$, $\tilde{\boldsymbol{P}}_{\mathrm{x}}$ and $\tilde{\boldsymbol{P}}_{\mathrm{sp}}$ are explained in the next sections.

4.2.1 Zero-crossing precoding

In this section we describe the process to obtain the vector $\tilde{\boldsymbol{p}}_{\mathrm{x}_k}$ which is the temporal precoded vector for user k. Given that the process is identically distributed and independent for each user and for the real and imaginary parts of $\tilde{\boldsymbol{x}}$ the development shown below is only described for a single user and for the real part of $\tilde{\boldsymbol{x}}$, that is $\boldsymbol{x} = \mathrm{Re}\left\{\tilde{\boldsymbol{x}}\right\}$.

Once we have the input symbol sequence $\boldsymbol{x}$, the sequence of samples $\boldsymbol{c}_{\mathrm{out}}$ is generated, as it is described in the Section 3.5. The sequence c_{out} which conveys the information in the zero-crossing time instances is taken as the input vector for solving the convex waveform optimization problem as described below.

4.2.2 Waveform design optimization

In general, samples close to the decision threshold are more sensitive to noise, so the waveform design optimization is addressed through the precoding optimization to maximize the minimum absolute value of the receive signal $\boldsymbol{y}$ in the noise-free environment, prior to the quantization process. In the optimization process the sign of the receive signal $\boldsymbol{y}$ is constrained to be equal to c_{out}. In other words, we maximized γ such that the samples have a maximum distance to the decision threshold and $\boldsymbol{z}$ be as close as possible to $\boldsymbol{c}_{\mathrm{out}}$. In Fig. 4.2 is shown an example of the receive signal $\boldsymbol{y}$ before and after the quantization together with the minimum amplitude value γ.

Stemming from above, in this section the optimization process is described to obtain the optimal temporal precoding vector $\boldsymbol{p}_{\mathrm{x}}$. The corresponding equivalent optimization problem, similar to the ones in [11, 18], can be expressed in the epigraph form, cf. Section 4.1.3 in [19], with

$$
\begin{aligned}
\text{minimize:} \quad & \boldsymbol{a}^{\mathrm{T}}\boldsymbol{r}_{\mathrm{k}} \\
\text{subject to:} \quad & \boldsymbol{B}_{\mathrm{k}}\boldsymbol{r}_{\mathrm{k}} \leq 0 \\
& \left(\boldsymbol{W}\boldsymbol{r}_{\mathrm{k}}\right)^{\mathrm{T}}\left(\boldsymbol{W}\boldsymbol{r}_{\mathrm{k}}\right) \leq \frac{E_0}{2N_{\mathrm{u}}},
\end{aligned}
\tag{4-4}
$$

where

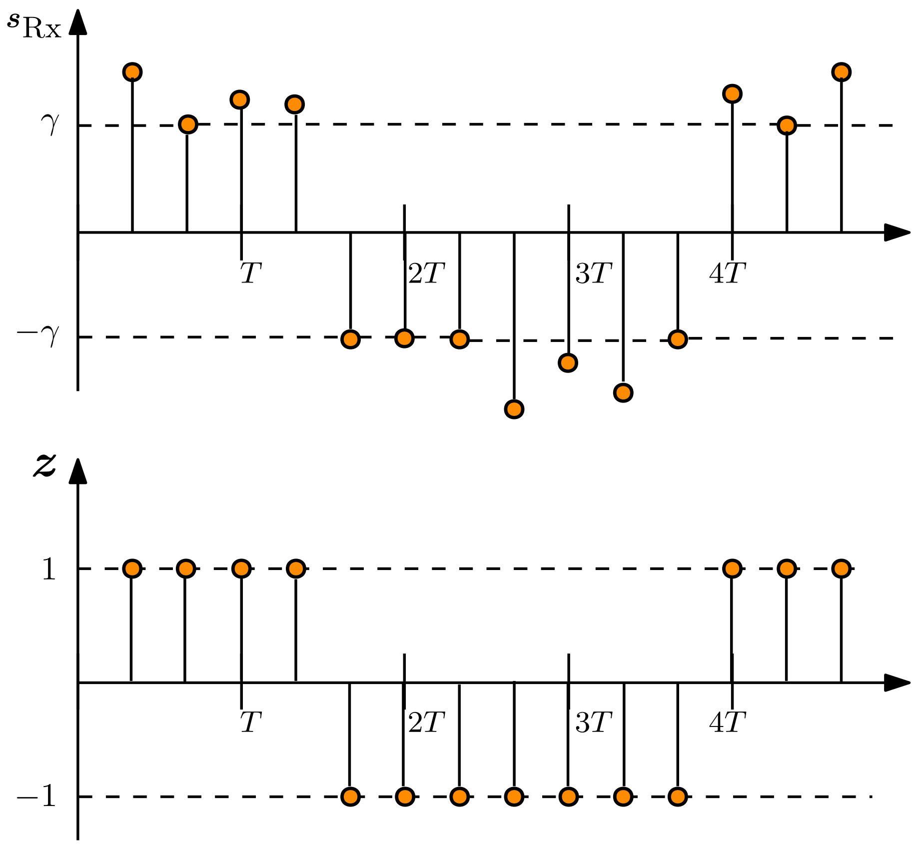

Figure 4.2: Example of the receive signal $\boldsymbol{y}$, the quantized signal $\boldsymbol{z}$ for $M_{\mathrm{Rx}} = 3$ and the minimum amplitude value γ in a noise-free environment

$$
\begin{aligned}
\boldsymbol{r}_{\mathrm{k}} &= \left[\boldsymbol{p}_{\mathrm{x_k}}^T, -\gamma\right]^{\mathrm{T}} \\
\boldsymbol{a} &= \left[\boldsymbol{0}_{1\times N_{\mathrm{q}}}, 1\right]^{\mathrm{T}} \\
\boldsymbol{B}_{\mathrm{k}} &= -\left[\beta \boldsymbol{C}_{\mathrm{k}} \boldsymbol{V}\boldsymbol{U}, \boldsymbol{1}_{N_{\mathrm{tot}}\times 1}\right] \\
\boldsymbol{C}_{\mathrm{k}} &= \mathrm{diag}\left(\boldsymbol{c}_{\mathrm{out_k}}\right) \\
\boldsymbol{W} &= \left[\boldsymbol{G}_{\mathrm{Tx}}^T \boldsymbol{U}, \boldsymbol{0}_{N_{\mathrm{tot}}\times 1}\right].
\end{aligned}
\tag{4-5}
$$

The cost function to be maximized is defined by $\boldsymbol{r}_k$ which contains the temporal precoding vector and the distance to the decision threshold γ with negative sign. The first constraint $\boldsymbol{B}$ addresses the optimization problem to maximize the minimum distance to the decision threshold in the desired direction induced by $\boldsymbol{c}_{\mathrm{out}}$. The second constraint with $\boldsymbol{W}$ accounts for the transmit energy constraint. Unlike the problem formulation in [11], the energy constraint in (4-4) explicitly takes into account $g_{\mathrm{Tx}}(t)$ as the sequence $\boldsymbol{p}_{\mathrm{x}}$ does not have a white power spectrum for the considered cases.

Moreover, the problem is a convex QCQP given that the objective function is convex and is minimized over a convex feasible set.

The optimization problem defined in (4-4) can be classified as a quadratically constrained quadradic program (QCQP) since the objective is linear and the constraints are linear and quadratic, respectively. Moreover, the problem is a convex QCQP given that the objective function is convex and is minimized over a convex feasible set. Additionally it is also defined as a QCQP since $\boldsymbol{W}^{\mathrm{T}}\boldsymbol{W} \in S_{+}^{n}$ (cf. Section 4.4 in [19]).

Implicitly, the optimization problem shapes the waveform $y(t)$ at the receiver, which is described in the discrete model by $\beta\boldsymbol{V}\boldsymbol{U}\boldsymbol{p}_{\mathrm{x}}$ for the noiseless case, where β is a signal gain provided by the spatial channel precoder.

The described convex optimization problem is solved for each user k having into account the desired output pattern $\boldsymbol{c}_{\mathrm{out}_k}$.

Finally, the matrix $\tilde{\boldsymbol{P}}_{\mathrm{x}}$ is formed by stacking the signal $\boldsymbol{V}\boldsymbol{U}\boldsymbol{p}_{\mathrm{x}_k}$ for all the users in the following way:

$$\tilde{\boldsymbol{P}}_{\mathrm{x}} = \left[(\boldsymbol{V}\boldsymbol{U}\tilde{\boldsymbol{p}}_{\mathrm{x}_1})^{\mathrm{T}}; (\boldsymbol{V}\boldsymbol{U}\tilde{\boldsymbol{p}}_{\mathrm{x}_2})^{\mathrm{T}}; \ldots; (\boldsymbol{V}\boldsymbol{U}\tilde{\boldsymbol{p}}_{\mathrm{x}_{N_{\mathrm{u}}}})^{\mathrm{T}}\right], \tag{4-6}$$

where $\boldsymbol{U}$ and $\boldsymbol{V}$ are given by (3-8) and (3-9), respectively. The next section explains the ZF spatial channel precoder.

4.2.3 Spatial zero-forcing precoding

Assuming perfect channel state information the spatial ZF precoding matrix [20] is implemented, since it generates a received signal without interference. The ZF precoding does not have influence over the noise at the receiver, then all interference produced by the transmitter is avoided [21]. The zero-forcing precoding results from minimizing the MSE with transmit power constraint and under the design criterion of conditional unbiasedness [22].

The ZF precoding definition is given by :

$$\tilde{\boldsymbol{P}}_{\mathrm{sp}} = \tilde{\boldsymbol{P}}_{\mathrm{zf}} = c_{\mathrm{zf}}\tilde{\boldsymbol{H}}^{\mathrm{H}}\left(\tilde{\boldsymbol{H}}\tilde{\boldsymbol{H}}^{\mathrm{H}}\right)^{-1}, \tag{4-7}$$

where $c_{\mathrm{zf}} = 1/f$ is the normalization factor which scales the transmit filter to the total transmit power E_{Tx} such that for all users the same power value is allocated. To determine the normalization factor, we consider the temporal transmit signals, described in the matrix $\tilde{\boldsymbol{P}}_{\mathrm{x,Tx}}$, where the Toeplitz matrix $\boldsymbol{G}_{\mathrm{Tx}}^{T}$ is given in (3-11).

$$\tilde{\boldsymbol{P}}_{\mathrm{x,Tx}} = \left[(\boldsymbol{G}_{\mathrm{Tx}}^{T}\boldsymbol{U}\tilde{\boldsymbol{p}}_{\mathrm{x}_1})^{T}; (\boldsymbol{G}_{\mathrm{Tx}}^{T}\boldsymbol{U}\tilde{\boldsymbol{p}}_{\mathrm{x}_2})^{T}; \ldots; (\boldsymbol{G}_{\mathrm{Tx}}^{T}\boldsymbol{U}\tilde{\boldsymbol{p}}_{\mathrm{x}_{N_{\mathrm{u}}}})^{T}\right], \tag{4-8}$$

with the aforementioned and considering uncorrelated user signals the signal covariance matrix reads as

$$\boldsymbol{R} = \mathbb{E}\left\{\tilde{\boldsymbol{P}}_{\mathrm{x,Tx}}\tilde{\boldsymbol{P}}_{\mathrm{x,Tx}}^{\mathrm{H}}\right\} = E_{\mathrm{Tx}}\boldsymbol{I}_{N_{\mathrm{u}}}. \tag{4-9}$$

Taking into account the spatial precoding in (4-9) and considering $\frac{E_0}{E_{\mathrm{Tx}}} = N_\mathrm{u}$ as the energy allocated per each user, the total transmit energy can be cast as

$$E_0 = \mathrm{trace}\left(\tilde{\boldsymbol{P}}_{\mathrm{zf}} \boldsymbol{R} \tilde{\boldsymbol{P}}_{\mathrm{zf}}^{\mathrm{H}}\right), \tag{4-10}$$

then the ZF scaling factor yields

$$c_{\mathrm{zf}} = \sqrt{\frac{N_\mathrm{u}}{\mathrm{trace}\left(\left(\tilde{\boldsymbol{H}}\tilde{\boldsymbol{H}}^{\mathrm{H}}\right)^{-1}\right)}}. \tag{4-11}$$

For ZF precoding, $\tilde{\boldsymbol{H}}\tilde{\boldsymbol{P}}_{\mathrm{sp}} = \beta \boldsymbol{I}_{N_\mathrm{u}}$ where β refers to the real valued beamforming gain, which is equal to c_{zf}. This gain is given due to the coherent combining effect of the wirelesses signal at the transmitter, increasing the signal-to-noise ratio (SNR) therefore improving robustness against noise [16].

Considering β, the receive signal given by (4-3) simplifies to

$$\tilde{\boldsymbol{Z}} = \mathrm{Q}(\beta \tilde{\boldsymbol{P}}_{\mathrm{x}} + \tilde{\boldsymbol{N}} \boldsymbol{G}_{\mathrm{Rx}}^{T}), \tag{4-12}$$

and the received signal at the k-th user can be written as

$$\tilde{\boldsymbol{z}}_k = Q(\beta \boldsymbol{V}\boldsymbol{U}\tilde{\boldsymbol{p}}_{\mathrm{x}_k} + \boldsymbol{G}_{\mathrm{Rx}}\tilde{\boldsymbol{n}}_k), \tag{4-13}$$

where the vector $\tilde{\boldsymbol{n}}_k$ with length $3N_{\mathrm{tot}}$ contains i.i.d. complex Gaussian noise samples with zero mean and variance $\sigma_{\tilde{n}}^2$.

4.2.4 Detection

Since the waveform design scheme is made for 1-bit receivers in order to meet the requirements of low complexity devices, the detection process must be straightforward as possible. Hence, we are headed for an optimal alternative that allow very low complexity symbol detection.

Optimal detectors like maximum likelihood (ML) detection turn out to be impractical since each evaluation of the ML metric implies the solution of the convex optimization problem described in (4-4). Moreover, ML detection suffers from the issue that a large number of candidates have to be tested as the whole sequence has to be evaluated. Therefore, a simple detection process is favorable, in order to meet the requirements of low complexity devices.

As in the same case of the modulation process presented in Section 3.5 the real and imaginary parts of the received signal $\tilde{\boldsymbol{z}}_k$ are processed independently and identically. So the detection process is also formulated separately for each user k. Thus, the following describes the detection process for the real part of $\tilde{\boldsymbol{z}}$.

Given the used detector is based on the zero-crossing detection, the memory of the channel is limited to one previous sample only, corresponding to the last sample of the previous symbol, denoted by ρ_{i-1}.

At the detector the received signal (4-13) is divided into N subsequences of length $M_{\mathrm{Rx}}+1$ denominated $\boldsymbol{z}_{b,i}$, where the first sample of $\boldsymbol{z}_{b,i}$ corresponds to the last sample of the previous subsequence $\boldsymbol{z}_{b,i-1}$, this is $\hat{\rho}_{i-1}$ required to perform the backward mapping process $\overleftarrow{d} : \boldsymbol{z}_{b,i} \rightarrow \mathcal{X}_{\mathrm{in}}$. In the noise free case, the subsequences $\boldsymbol{z}_{b,i}$ are valid codewords that meet the requirements established in $\mathcal{C}_{\mathrm{map}}$.

Based on the structure of $\boldsymbol{z}_{b,i}$, in $\mathcal{C}_{\mathrm{det}}$ all the valid subsequences are collected, in the way $[\rho, \boldsymbol{c}_s]$ such that $\boldsymbol{z}_{b,i} \subseteq \mathcal{C}_{\mathrm{det}}$ and $\mathcal{C}_{\mathrm{det}}$ meet the requirements imposed in $\mathcal{C}_{\mathrm{map}}$. Table 4.1 shows the valid codewords $\mathcal{C}_{\mathrm{det}}$ for $M_{\mathrm{Rx}} = 3$ in a noise-free environment.

Table 4.1: $\mathcal{C}_{\mathrm{det}}$ for $M_{\mathrm{Rx}} = 3$, where the first $M_{\mathrm{Rx}}+1$ subsequences correspond to $\rho = 1$ and the last $M_{\mathrm{Rx}}+1$ subsequences to $\rho = -1$

$\mathcal{C}_{\mathrm{det}}$	
symbol	$\boldsymbol{c}_{\mathrm{det}}$
b_1	$1 \quad 1 \quad 1 \quad 1$
b_2	$1 \quad 1 \quad 1 \quad -1$
b_3	$1 \quad 1 \quad -1 \quad -1$
b_4	$1 \quad -1 \quad -1 \quad -1$
b_1	$-1 \quad -1 \quad -1 \quad -1$
b_2	$-1 \quad -1 \quad -1 \quad 1$
b_3	$-1 \quad -1 \quad 1 \quad 1$
b_4	$-1 \quad 1 \quad 1 \quad 1$

So, the subsequence $\boldsymbol{z}_{b,i}$ is searched in $\mathcal{C}_{\mathrm{det}}$ such that is backward mapped, through $\overleftarrow{d} : \boldsymbol{z}_{b,i} \rightarrow \mathcal{X}_{\mathrm{in}}$, into the corresponding symbol. The detection of the first symbol is made taking into account the pilot signal *pb*. In Fig. 4.3 an example about how the subsequences $\boldsymbol{z}_{b,i}$ are formed taking into account the pilot signal *pb* and the last sample of the previous subsequence $\hat{\rho}_{i-1}$ is depicted.

The above process is sufficient for establishing a unique detection in the noiseless environment. With this, it is possible to perform a perfect recovery of $\boldsymbol{x}$ only by considering the backward mapping process. However, the presence

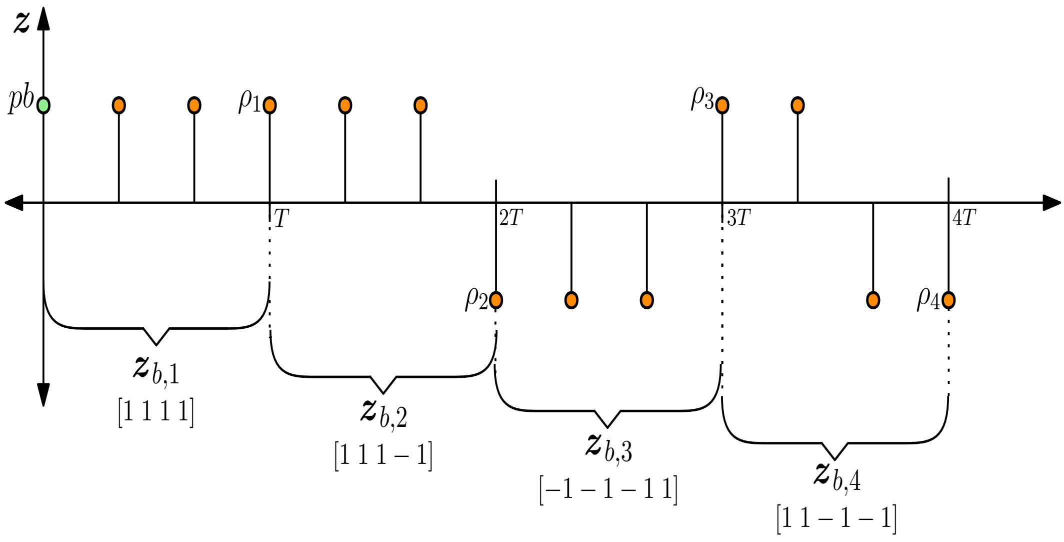

Figure 4.3: Representation of the $\boldsymbol{z}_{b,i}$ subsequences

of noise can alter the received samples in such a way that invalid codewords are generated such that they are not in $\mathcal{C}_{\text{det}}$. The latter means that $\boldsymbol{z}_{b,i} \nsubseteq \mathcal{C}_{\text{det}}$. Therefore, additional decision rules are defined in terms of consideration of the Hamming-distance metric [11].

For two codewords of equal length, the Hamming-distance is defined as the number of positions that have to be changed to convert one word into another. For this case the subsequence $\boldsymbol{z}_{b,i}$ is compared with all the valid sequences from $\mathcal{C}_{\text{det}}$ through the Hamming-distance, so that the valid codeword with minimum distance $\boldsymbol{c}$ is selected and the backward mapping process is carried out with the codeword $\boldsymbol{c}$. Thus, the i-th symbol is detected according to

$$\widehat{x_i} = \overleftarrow{d}\left(\boldsymbol{c}\right), \quad \text{where} \quad \boldsymbol{c} = arg \min_{\boldsymbol{c}_{\text{det}}} \ \text{Hamming}\left(\boldsymbol{z}_{b,i}, \boldsymbol{c}_{\text{det}}\right),$$

where Hamming $\left(\boldsymbol{z}_{b,i}, \boldsymbol{c}_{\text{det}}\right) = \sum_{n=1}^{M_{\text{Rx}}+1} \frac{1}{2} \left|\boldsymbol{z}_{b,i,n} - \boldsymbol{c}_{\text{det},n}\right|$.

4.2.5
Simulation results

The BER performance curves shown below result from the simulations of the discrete system model described in (4-12) and (4-13) with different oversampling factors M_{Rx} and different signaling factors M_{Tx}. The Tx and Rx filters are described by (3-1) and (3-3), respectively both with parameter T_s for pulse duration and roll-off factor $\epsilon_{\text{Rx}} = \epsilon_{\text{Tx}} = 0.22$ and bandwidth $W_{\text{Rx}} = W_{\text{Tx}} = (1 + \epsilon_{\text{Tx}})\,/T_{\text{s}}$.

The simulation results show the performance of the MMDDT precoding method described in this chapter, which conveys the information in the zero-crossing time instances of the received signal and is compared with the state-of-the-art [11] . For the simulation of the state-of the-art, it was considered the same data rates and a bandwidth constraint incorporated only by the pulse shaping filter. In order to provide the same conditions, both approaches were analyzed under the same input sequence $\tilde{\boldsymbol{x}}$ but considering, for [11], solving the convex optimization problem (4-4) with the desired output pattern $\boldsymbol{c}_{\text{out}}$ given by the optimized forward mapping scheme devised in [11]. Together with the approaches mentioned above, a common QPSK modulated signal is presented as a reference, corresponding to only 2 bits per time interval T.

The signal-to-noise ratio for numerical evaluation of the uncoded BER is defined as

$$\text{SNR} = \frac{E_0/(N_{\text{q}}T)}{N_0\,(1+\epsilon_{\text{Rx}})\,\frac{1}{T}} = \frac{E_0}{N_{\text{q}}N_0\,(1+\epsilon_{\text{Rx}})}, \tag{4-14}$$

where N_0 represents the complex noise power density. The length of the sequence $\tilde{\boldsymbol{x}}_{\text{k}}$ is set to $N = 50$ symbols, the number of transmit antennas to $N_{\text{t}} = 50$ and the number of users to $N_{\text{u}} = 5$. The used channel for the numerical results is the channel described in Section 4.1 under the following parameters

$$\begin{aligned} r_d &= 1000 \text{ mts} \\ d &= 300 \text{ mts} \\ \sigma_{\text{shadow}} &= 8 \text{ dB} \\ \nu &= 3. \end{aligned} \tag{4-15}$$

The BER performance for different sampling rate and signaling rate ($\frac{M_{\text{Rx}}}{T}$, $\frac{M_{\text{Tx}}}{T}$) for the proposed MMDDT precoding and the approach presented in [11], can be seen in Fig. 4.4, both with spatial precoding ZF.

The curves depicted in Fig. 4.4 showed that the proposed ZC precoding has a better performance in terms of BER than the state-of-the-art method [11]. Among all the considered cases the configuration with $M_{\text{Rx}} = M_{\text{Tx}} = 2$ presents the best performance overcoming the best case of [11], given with $M_{\text{Rx}} = M_{\text{Tx}} = 3$.

In Table 4.2 is shown the average value for γ obtained in the simulations performed for all the configurations of Fig. 4.4, being for $M_{\text{Rx}} = M_{\text{Tx}} = 2$ the configuration that yields the highest average value for γ. Likewise, Table 4.3 compares the numbers of zero-crossings, in reference to $\boldsymbol{c}_{\text{out}}$, occurring in both approaches, obtaining that the number of zero-crossings is lower for the zero-crossing approach proposed in this work. Considering a lowpass characteristic of $v(t)$, the optimization problem in (4-4) becomes more difficult

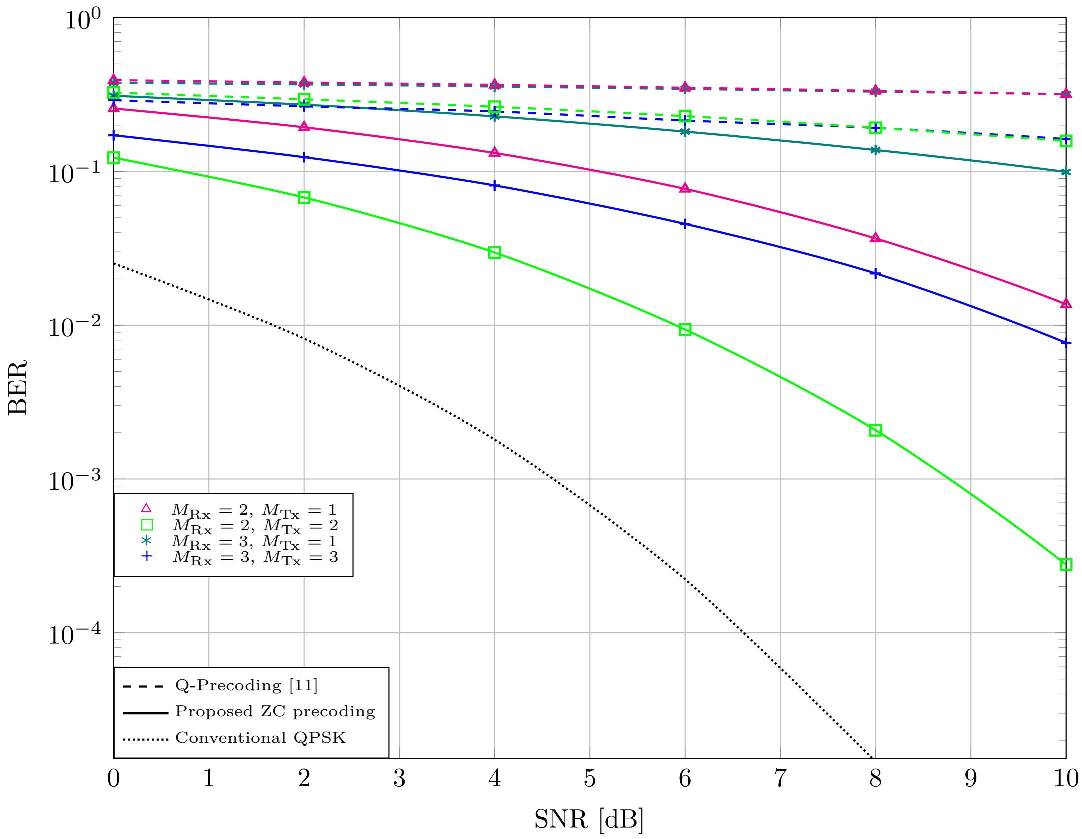

Figure 4.4: BER versus SNR for different M_{Rx} and M_{Tx}. Fixed parameters are $N = 50$, $N_{\mathrm{t}} = 50$ and $N_{\mathrm{u}} = 5$.

with introducing zero-crossings. In return, a reduced number of zero-crossings can simplify the problem and can yield a higher value for γ.

In addition, in Fig. 4.5 is shown the power spectral density (PSD) for the considered waveforms. The results in Fig. 4.5 were simulated with the same configurations presented in Fig. 4.4 employing (4-16)

$$\mathrm{PSD}_{[\mathrm{dB}]} = 10\log_{10}\left[\left|\frac{F_k}{\sqrt{3N_{\mathrm{tot}}}}\right|^2\right], \tag{4-16}$$

where F_k is the discrete Fourier transform (DFT) of the transmit signal given by

$$\tilde{\boldsymbol{s}}_{\mathrm{Tx},k} = (\boldsymbol{G}_{\mathrm{Tx}}^T \boldsymbol{U} \tilde{\boldsymbol{p}}_{\mathrm{x}_k})^T. \tag{4-17}$$

Table 4.2: Comparison of γ statistics between the ZC-Precoding and Q-precoding [11] approaches

	Q-Precoding [11]		ZC Precodig	
	$\mathbb{E}\{\gamma\}$	$\mathbb{E}\left\{(\gamma - \mathbb{E}\{\gamma\})^2\right\}$	$\mathbb{E}\{\gamma\}$	$\mathbb{E}\left\{(\gamma - \mathbb{E}\{\gamma\})^2\right\}$
$M_{\text{Rx}} = 2,\ M_{\text{Tx}} = 1$	0.0018	1.2612e-06	0.0176	1.3568e-06
$M_{\text{Rx}} = 2,\ M_{\text{Tx}} = 2$	0.0054	2.3568e-06	0.0211	1.1192e-06
$M_{\text{Rx}} = 3,\ M_{\text{Tx}} = 3$	0.0030	4.8885e-07	0.0100	2.3662e-07
$M_{\text{Rx}} = 3,\ M_{\text{Tx}} = 1$	4.9369e-04	1.3975e-07	0.0076	4.9079e-07

Table 4.3: Average number of zero-crossings per unit time interval T

	Q-Precoding [11]	ZC Precoding
$M_{\text{Rx}} = 2$	0.758	0.625 (5/8 cf. Table 3.6)
$M_{\text{Rx}} = 3$	0.86	0.75 (3/4 cf. Table 3.4)

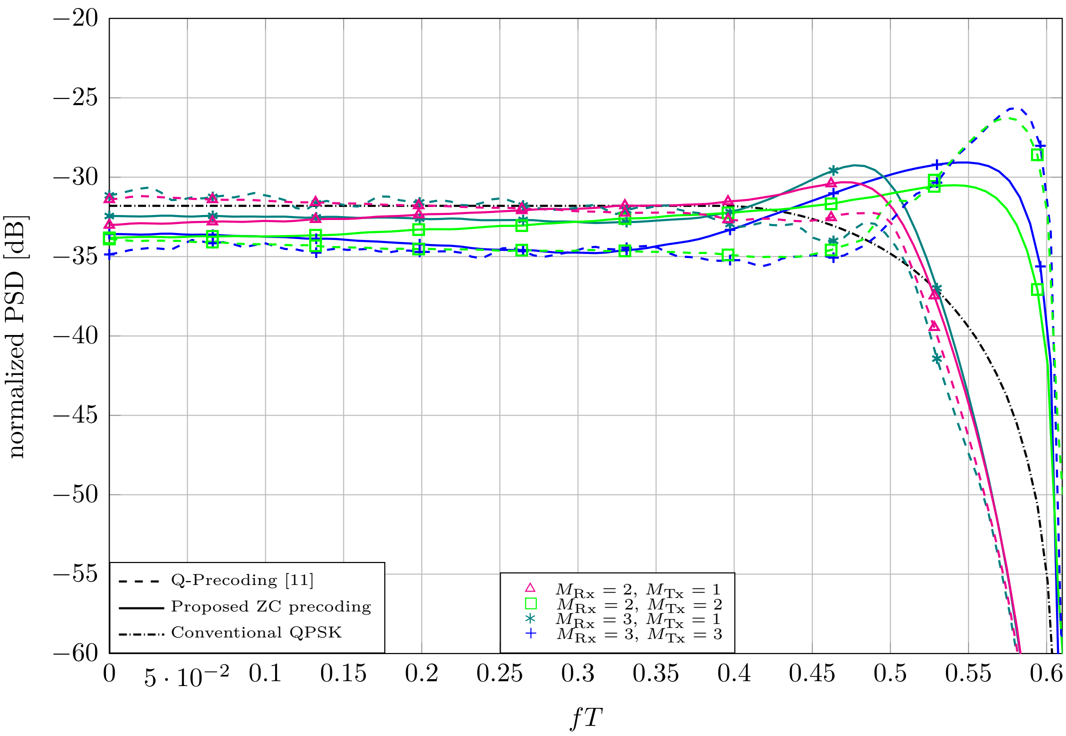

Figure 4.5: Power spectral density for the experiment in Fig. 4.4.

Simulations were also performed to observe the influence of the bandwidth symbol duration (varying T_s) on γ. For this it is necessary to introduce the D-fold higher sampling rate which allows to model the effects of aliasing that occur at the receiver due to increased bandwidth. Thus the waveform response $\boldsymbol{v} = \boldsymbol{D}\boldsymbol{v}'$ is given by the convolution of the transmit and receive filter, both with D-fold sampling rate $\frac{MDM_{\text{Tx}}}{T}$ and then the waveform response represented by the vector response $\boldsymbol{v}'$ is D-fold decimated by the multiplication with the matrix $\boldsymbol{D}$ defined as

$$\boldsymbol{D}_{m,n} = \begin{cases} 1, & \text{for} \quad n = (m-1)\,D + 1 \\ 0, & \text{else,} \end{cases} \tag{4-18}$$

where the matrix $\boldsymbol{D}$ has dimensions $L \times (LD - D + 1)$ with L being the length of the vector $\boldsymbol{v}$.

In Fig. (4.6) it is depicted the γ results under the influence of the bandwidth. The results show that, for the zero-crossing approach and the one presented in [11], with a large bandwidth γ is limited only by the transmit energy and γ tends to zero with decreasing the bandwidth. As it was expected, the zero-crossing approach provides a larger distance to the decision threshold when reducing bandwidth as compared to the forward mapping in [11] besides γ tends to reach the same value for both approaches with a large bandwidth. The case for $W_{\mathrm{Tx}}T = 1$ supports the theory that $\log_2(M_{\mathrm{Rx}} + 1)$ bits per Nyquist interval can be transmitted in the noise-free case [3], and that there is a reasonable tolerance against noise.

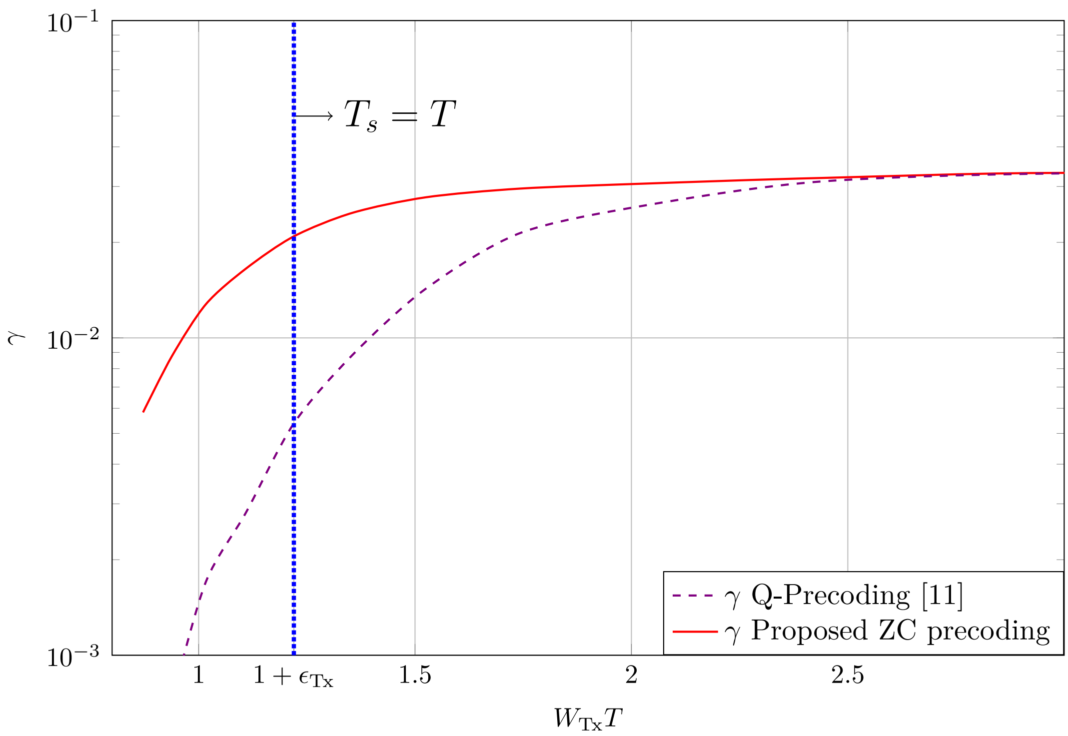

Figure 4.6: γ vs bandwidth for $M_{\mathrm{Rx}} = M_{\mathrm{Tx}} = 2$

4.3 MMSE spatio-temporal precoding

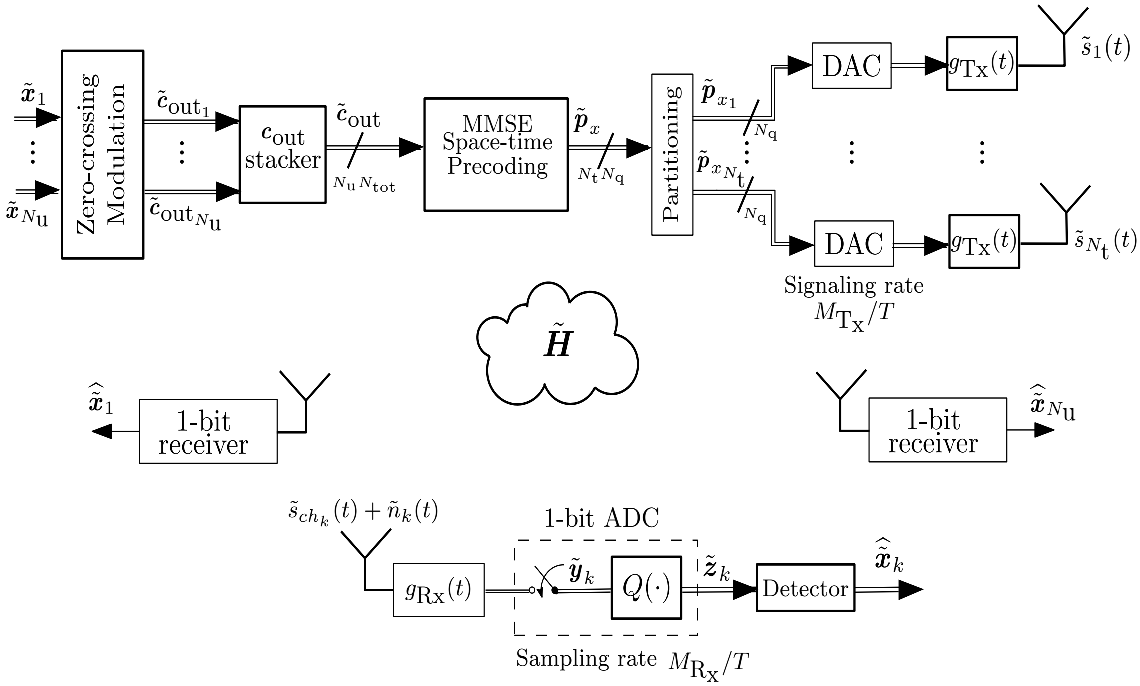

Figure 4.7: Multiuser MIMO system model with MMSE Spatio-temporal precoding

A multiuser MIMO downlink channel with N_t transmit antennas at the BS and N_u single antenna users is considered as presented in Fig. 4.7. The input block symbol sequence associated to the kth user is given by $\tilde{\boldsymbol{x}}_k$ with N complex symbols and $k = 1, \ldots, N_u$. In the sequel each $\tilde{\boldsymbol{x}}_k$ sequence is fed into the zero-crossing modulator to be mapped in the desired output pattern $\tilde{\boldsymbol{c}}_{\text{out},k}$ for further processing.

In the system the signaling rate $\frac{M_{\text{Tx}}}{T}$ and the sampling rate $\frac{M_{\text{Rx}}}{T} = \frac{M M_{\text{Tx}}}{T}$ is characterized by the transmit filter with impulse response $g_{\text{Tx}}(t)$ and the receive filter with impulse response $g_{\text{Rx}}(t)$, respectively. The combined waveform, determined by the transmit and receive filter, is given by the convolution of both filters $v(t) = g_{\text{Tx}}(t) * g_{\text{Rx}}(t)$.

At the receiver, the quantized sample block $\tilde{\boldsymbol{z}}_k$ for the kth user has a length of $N_{\text{tot}} = M_{\text{Rx}} N + 1$ samples. Stacking the received sequences of the N_u users yields the vector $\tilde{\boldsymbol{z}}$ with length $N_u N_{\text{tot}}$ given by

$$
\begin{aligned}
\tilde{\boldsymbol{z}} =& Q_1\left(\tilde{\boldsymbol{y}}\right) \\
=& Q_1\left(\left(\tilde{\boldsymbol{H}} \otimes \boldsymbol{I}_{N_{\mathrm{tot}}}\right)\left(\boldsymbol{I}_{N_{\mathrm{t}}} \otimes \boldsymbol{V}\boldsymbol{U}\right)\tilde{\boldsymbol{p}}_x + \left(\boldsymbol{I}_{N_{\mathrm{u}}} \otimes \boldsymbol{G}_{\mathrm{Rx}}\right)\tilde{\boldsymbol{n}}\right) \\
=& Q_1\left(\tilde{\boldsymbol{H}}_{\mathrm{eff}}\tilde{\boldsymbol{p}}_x + \boldsymbol{G}_{\mathrm{Rx,eff}}\tilde{\boldsymbol{n}}\right),
\end{aligned}
\qquad (4\text{-}19)
$$

where $Q(\cdot)$ is the 1-bit quantizer described in (3-6) and the channel matrix $\tilde{\boldsymbol{H}}$ of size $N_{\mathrm{u}} \times N_{\mathrm{t}}$ is the same as that described in Section 4.1. The waveform impulse response matrix $\boldsymbol{V}$, the receive filter matrix $\boldsymbol{G}_{\mathrm{Rx}}$ and the M-fold upsampling matrix $\boldsymbol{U}$ are given by equations (3-9), (3-10) and (3-8), respectively. The vector $\tilde{\boldsymbol{n}}$ with length $3N_{\mathrm{tot}}N_{\mathrm{u}}$ represents the complex Gaussian noise vector with zero mean and variance σ_n^2.

The space-time precoding vector $\tilde{\boldsymbol{p}}_x$ with length $(N_{\mathrm{T}}N_{\mathrm{q}})$, where $N_{\mathrm{q}} = M_{\mathrm{Tx}}N + 1$, is computed based on the stacked desired output pattern $\tilde{\boldsymbol{c}}_{\mathrm{out}}$.

As for the precoder proposed in Chapter 4 the first step to design the MMSE precoder is to built the sequence $\tilde{\boldsymbol{c}}_{\mathrm{out}_k}$ which conveys the information in the time instance of the zero-crossing. The pattern $\tilde{\boldsymbol{c}}_{\mathrm{out}_k}$ is obtained independently and equally for each of the k users as well as for the real and imaginary parts of the input sequence $\tilde{\boldsymbol{x}}_k$. So, for the development of the MMSE spacial-temporal precoding, the modulation procedure described in Section 3.5 is used.

The sequence $\tilde{\boldsymbol{c}}_{\mathrm{out}}$ is obtained by stacking, in one single vector, the pattern $\tilde{\boldsymbol{c}}_{\mathrm{out}_k}$ of each user so that

$$
\tilde{\boldsymbol{c}}_{\mathrm{out}} = [\tilde{\boldsymbol{c}}_{\mathrm{out}_1}^T, ..., \tilde{\boldsymbol{c}}_{\mathrm{out}_k}^T, ..., \tilde{\boldsymbol{c}}_{\mathrm{out}_{N_{\mathrm{u}}}}^T]^T \qquad (4\text{-}20)
$$

The next subsection explains the MMSE design to get the space-time precoding vector $\tilde{\boldsymbol{p}}_{\mathrm{x}}$, once the desired output pattern $\tilde{\boldsymbol{c}}_{\mathrm{out}}$ is obtained.

4.3.1 MMSE design

In this section the optimal solution of $\tilde{\boldsymbol{p}}_{\mathrm{x}}$ according to the MSE criterion is presented where a maximum total transmit energy E_0 is considered. The linear MMSE precoder minimizes the mean square error between the receive signal $\tilde{\boldsymbol{z}}$ and the desired output pattern $\tilde{\boldsymbol{c}}_{\mathrm{out}}$ under a total transmit power constraint [22].

Based on [21] we follow a similar approach considering a scaling factor in the MMSE problem formulation. The design of the space-time MMSE precoder can be formulated as (4-21) taking into account the desired output pattern $\tilde{\boldsymbol{c}}_{\mathrm{out}}$ at the receiver,

$$\begin{aligned} \min_{f,\tilde{\boldsymbol{p}}_{\mathrm{x}}} \quad & \mathrm{E}\{\|f(\tilde{\boldsymbol{H}}_{\mathrm{eff}}\tilde{\boldsymbol{p}}_{\mathrm{x}} + \boldsymbol{G}_{\mathrm{Rx,eff}}\tilde{\boldsymbol{n}}) - \tilde{\boldsymbol{c}}_{\mathrm{out}}\|_2^2\} \\ \text{subject to:} \quad & \tilde{\boldsymbol{p}}_{\mathrm{x}}^H \boldsymbol{A}^H \boldsymbol{A} \tilde{\boldsymbol{p}}_{\mathrm{x}} \leq E_0, \end{aligned} \tag{4-21}$$

with

$$\boldsymbol{A} = \left(\boldsymbol{I}_{N_{\mathrm{t}}} \otimes \boldsymbol{G}_{\mathrm{Tx}}^T \boldsymbol{U}\right) \tag{4-22}$$

and $\boldsymbol{G}_{\mathrm{Tx}}$ beign the Toeplitz matrix described in (3-11).

By exploiting the knowledge that the optimal precoding vector must fulfill the total energy constraint with equality, the objective function in (4-21) can be solved in closed form even if this is not a convex problem e.g., by [21].

The optimal solution of (4-21) is given as

$$\tilde{\boldsymbol{p}}_{\mathrm{x,opt}} = \frac{1}{f}\left(\tilde{\boldsymbol{H}}_{\mathrm{eff}}^H \tilde{\boldsymbol{H}}_{\mathrm{eff}} + \frac{\mathrm{trace}\{\boldsymbol{G}_{\mathrm{Rx}}^H \boldsymbol{C}_n \boldsymbol{G}_{\mathrm{Rx}}\}}{E_0} \boldsymbol{A}^H \boldsymbol{A}\right)^{-1} \tilde{\boldsymbol{H}}_{\mathrm{eff}}^H \tilde{\boldsymbol{c}}_{\mathrm{out}}, \tag{4-23}$$

$$= \frac{1}{f} \tilde{\boldsymbol{P}}_{\mathrm{SpT\text{-}MMSE}}\ \tilde{\boldsymbol{c}}_{\mathrm{out}} \tag{4-24}$$

where the scaling factor is defined by

$$f = \sqrt{\frac{\tilde{\boldsymbol{c}}_{\mathrm{out}}^H \tilde{\boldsymbol{\Gamma}} \tilde{\boldsymbol{c}}_{\mathrm{out}}}{E_0}}. \tag{4-25}$$

The MMSE spatio-temporal precoder derivation and the description of $\tilde{\boldsymbol{\Gamma}}$ are specified in the appendix section.

4.3.2 Detection

As mentioned in Section 4.2.4, one of the main requirements of the waveform design scheme for 1-bit receivers is the use of low complexity devices, therefore the detection process is aimed to be as straightforward as possible.

Since the received signal $\tilde{\boldsymbol{z}}$ is a vector that stacks the information received for all users, the first step to perform the detection process is to obtain the $\tilde{\boldsymbol{z}}_k$ signal for each user to later develop the corresponding backward mapping process $\overleftarrow{d}$ that is the inverse process of the zero-crossing modulation described in Section 3.5.

Once the $\tilde{\boldsymbol{z}}_k$ sequence is obtained, it is divided into segments $\tilde{\boldsymbol{z}}_{b_i}$ of length $M_{\text{Rx}}+1$ and together with $\hat{\rho}_{i-1}$, $\mathcal{C}_{\text{map}}$ and $\mathcal{C}_{\text{det}}$ the process is developed in the same way as it was described in Section 4.2.4 with the Hamming-distance metric.

Also, the the pilot signal $\hat{pb}$ enables the detection process for the detection of the first symbol in the sequence, then the sub-sequence $\tilde{\boldsymbol{z}}_{b_1}$ is constructed taking into account $\hat{pb}$.

For the detection of $\tilde{\boldsymbol{z}}$ the process is identical for each user and independent for the real and imaginary parts of $\tilde{\boldsymbol{z}}$ then it is realized separately just like the process to get $\tilde{\boldsymbol{c}}_{\text{out}}$, and the detection process for the MMDDT precoding described in Section 4.2.4.

The simulation results are shown below of the proposed MMSE spatial-temporal precoder with zero-crossing modulation that was described in this chapter.

4.3.3 Simulation results

The numerical evaluation of the spatial-temporal proposed zero-crossing precoding with MMSE and the FM known from the literature [11] in terms of the BER and MSE are presented in this section. The simulations were carried out for different values of M_{Rx} and M_{Tx} and it was also considered input sequences of length $N = 50$ and maximum energy constraint of $E_0 = 1$.

The transmit pulse shaping filter is a RC filter with roll-off factor $\epsilon_{\text{Tx}} = 0.22$ with impulse response given by (3-1). The receive pulse shaping filter on the other hand is an RRC filter with roll-off factor $\epsilon_{\text{Tx}} = 0.22$ and impulse response given by (3-3). The bandwidth is defined through $W_{\text{Rx}} = W_{\text{Tx}} = (1+\epsilon_{\text{Tx}})/T_{\text{s}}$. The number of transmit antennas is set to $N_{\text{t}} = 10$ and the number of users to $N_{\text{u}} = 2$. As it was mentioned earlier, the channel matrix $\tilde{\boldsymbol{H}}$ is the one detailed in Section 4.1 whose channel parameters are configured as follows:

$$\begin{aligned} r_d &= 1000 \text{ mts} \\ d &= 300 \text{ mts} \\ \sigma_{\text{shadow}} &= 8 \text{ dB} \\ \nu &= 3 \end{aligned} \tag{4-26}$$

The SNR is defined by (4-14), where N_0 denotes the complex noise power density.

As with the MMDDT precoder from Section 4.2, the MMSE precoder detailed in this chapter is also compared with the state-of-the-art [11] under the same input bit sequences and with the same bandwidth. For the FM precoding proposed in [11] the problem in (4-21) takes into account the desired output pattern $\boldsymbol{c}_{\text{out}}$ built according to the FM scheme developed in [11] but with the same MMSE space-time precoding approach. Given the complexity to solve (4-21) it was resolved to use the same input sequences $\tilde{\boldsymbol{x}}$ that were used for the MMDDT precoder together with the codebook selected for the FM approach (so that γ was maximized) avoiding to solve (4-21) for each codebook as is performed in [11].

Both approaches are evaluated for different values of M_{Rx} and M_{Tx} as can be observed in the Fig. 4.8

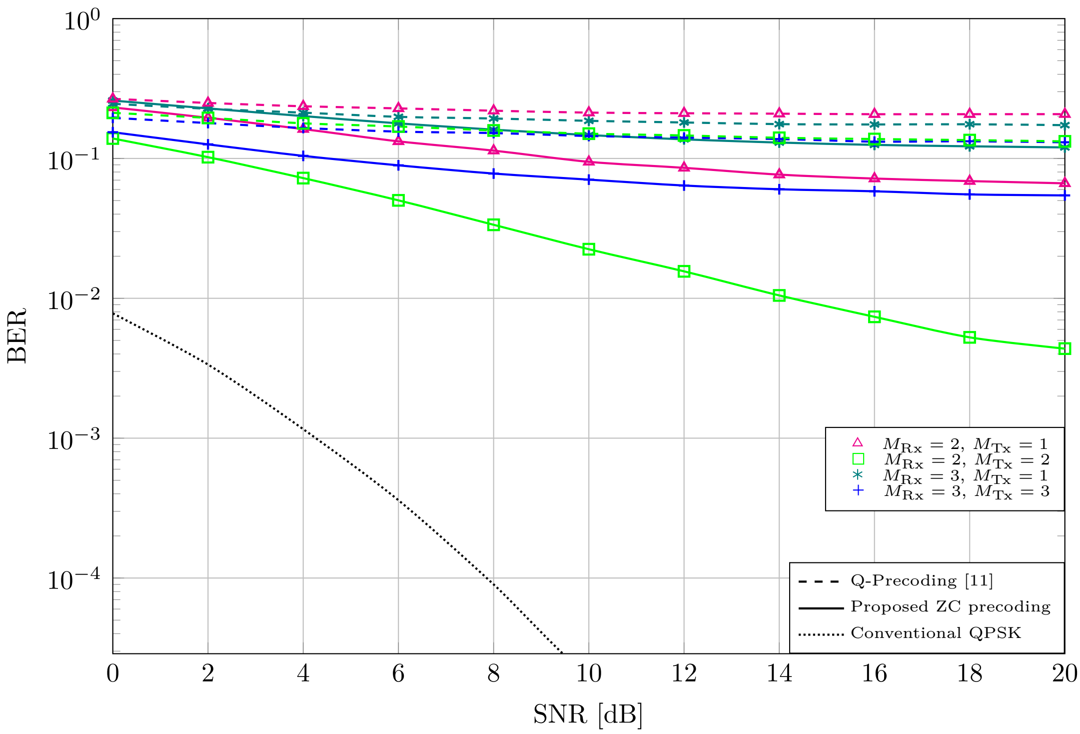

Figure 4.8: BER versus SNR for different M_{Rx} and M_{Tx}. Fixed parameters are $N = 50$, $N_{\text{t}} = 10$ and $N_{\text{u}} = 2$.

In the results shown in Fig. 4.8 the MMSE precoder based on zero-crossing modulation has better performance in terms of BER than the MMSE precoder with the FM approach proposed in [11]. The setting of $M_{\text{Rx}} = M_{\text{Tx}} = 2$ of the zero-crossing scheme is the configuration that presents the best overall performance. Besides a conventional QPSK modulated signal is presented as a reference.

For the same configuration set presented in Fig. 4.9, Fig. 4.9 illustrates the corresponding MSE cost function defined as:

$$
\begin{aligned}
J =& f^2 \tilde{\boldsymbol{p}}_{\mathrm{x}}^H \tilde{\boldsymbol{H}}_{\mathrm{eff}}^H \tilde{\boldsymbol{H}}_{\mathrm{eff}} \tilde{\boldsymbol{p}}_{\mathrm{x}} - 2f \mathrm{Re}\{\tilde{\boldsymbol{p}}_{\mathrm{x}}^H \tilde{\boldsymbol{H}}_{\mathrm{eff}}^H \tilde{\boldsymbol{c}}_{\mathrm{out}}\} \\
&+ f^2 \mathrm{trace}\{\boldsymbol{G}_{\mathrm{Rx,eff}} \boldsymbol{C}_n \boldsymbol{G}_{\mathrm{Rx,eff}}{}^H\},
\end{aligned} \tag{4-27}
$$

being $M_{\mathrm{Rx}} = M_{\mathrm{Tx}} = 2$ the set with the lowest MSE.

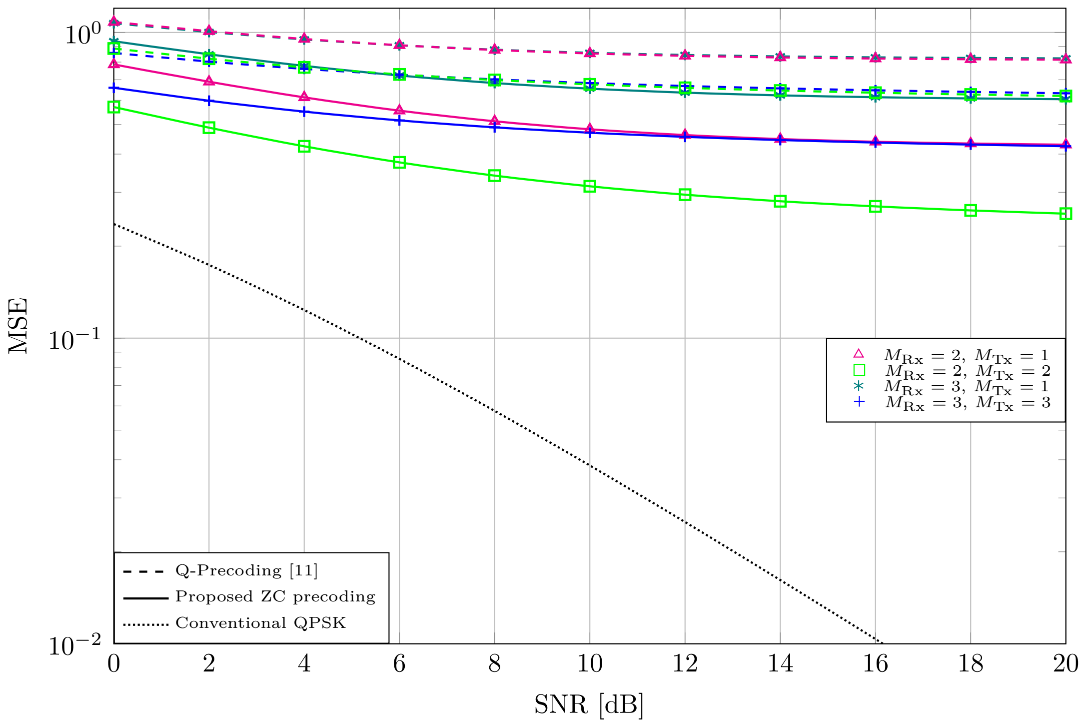

Figure 4.9: Cost function for the experiment in Fig. 4.8.

Moreover, in Fig. 4.10 it is shown PSD for the considered waveforms. The results in Fig. 4.10 were simulated with the same configurations presented in Fig. 4.8 employing (4-16) and (4-17). In this case F_k is the DFT from one transmit antenna.

Simulations were also performed to observe the influence of bandwidth on MSE. As in Section 4.2.5, matrix $\boldsymbol{D}$ is considered to model the effects of aliasing that occur when the bandwidth is increased.

In Fig. (4.6) the MSE versus bandwidth $W_{\mathrm{Tx}}T$ is illustrated for three different values of SNR. It can be seen that the MSE tends to decrease with the increase of the bandwidth. Moreover, it is shown that for both approaches, the zero-crossing precoding and the FM mapping from [11] tends to a similar value of MSE when the W_{Tx} goes to infinity. However, when the bandwidth is restricted as in the considered case, the proposed zero-crossing precoding

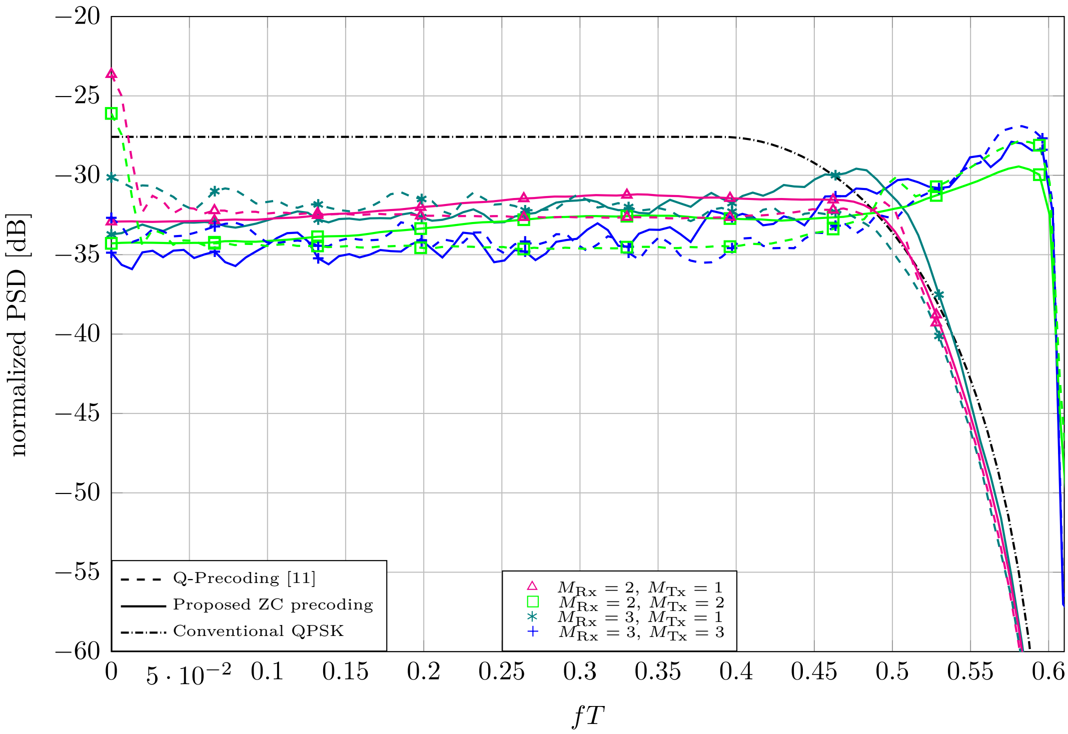

Figure 4.10: Power spectral density for the experiment in Fig. 4.8.

corresponds to a significantly lower MSE than the FM approach devised in [11].

In Fig. (4.11) is depicted the MSE results under the influence of the bandwidth. In general, it can be seen that for both approaches the MSE tends to decrease when the bandwidth is increased to the point when the W_{Tx} goes to infinity, that the zero-crossing precoding and the FM mapping from [11] reaches a similar value. Nevertheless, the proposed MMSE precoder with zero-crossing modulation corresponds to a significantly lower MSE than the FM approach presented in [11] when the bandwidth is restricted as in the numerical evaluations presented before.

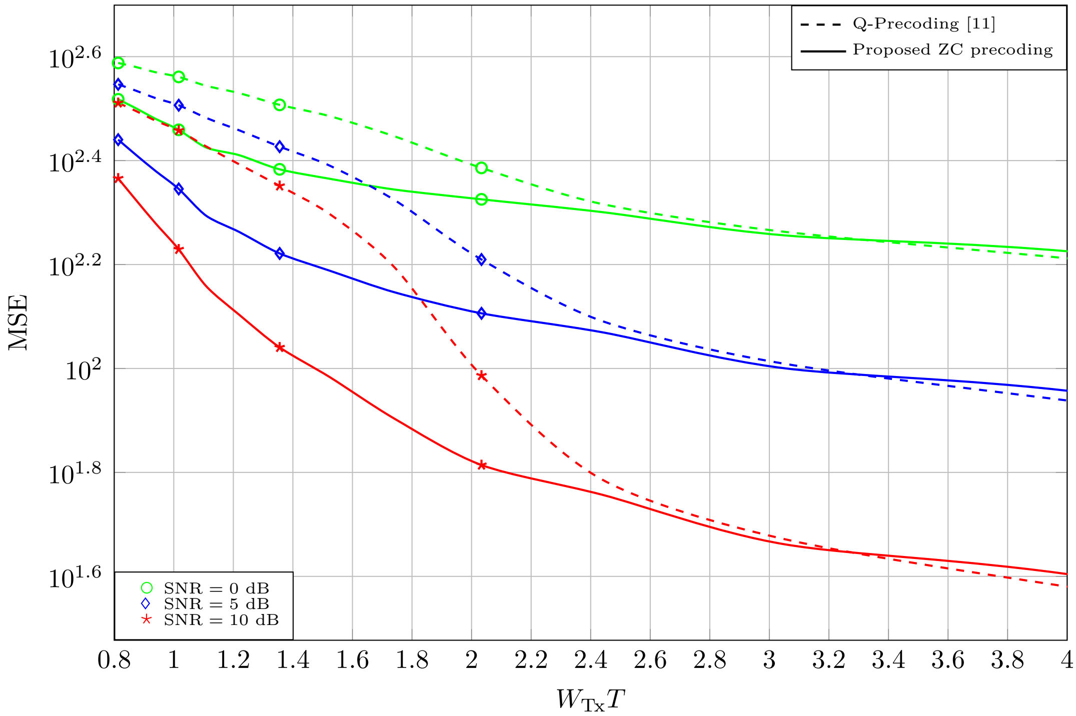

Figure 4.11: MSE vs bandwidth for $M_{\mathrm{Rx}} = M_{\mathrm{Tx}} = 2$ and different values of SNR

5
Inter-block-interference

Effects that occur in communications systems degrade the performance of the systems such as interblock interference (IBI) caused by the filters tails in a successive sequence transmission. To mitigate the IBI, it is necessary to insert a delay, known as a guard time interval between each transmit block. If this delay is known at the receiver it is possible to reduce the IBI and its effects over the system performance.

In this work we have studied the effects of IBI for the precoders based on zero-crossing: MMDDT together with ZF and the spatio-temporal precoding with MMSE. Experiments were carried out to determine the BER taking into account IBI where the l-th transmitted block is corrupted by neighboring blocks. To reduce the IBI the guard interval C_g is considered between the blocks.

In the next section it is described the model of IBI for the MMDDT precoding with ZF.

5.1
MMDDT IBI

Considering the transmission of l blocks, the received signal for the l blocks of the N_{u} user reads:

$$\tilde{\boldsymbol{Z}} = \mathrm{Q}(\tilde{\boldsymbol{H}}\tilde{\boldsymbol{P}}_{\mathrm{sp}}\tilde{\boldsymbol{P}}'_{\mathrm{x}} + \tilde{\boldsymbol{N}}\boldsymbol{G}^{T}_{\mathrm{Rx}}), \tag{5-1}$$

where

$$\tilde{\boldsymbol{P}}'_{\mathrm{x}} = \left[(\boldsymbol{V}'\boldsymbol{U}'\tilde{\boldsymbol{p}}'_{\mathrm{x}_1})^{\mathrm{T}}; (\boldsymbol{V}'\boldsymbol{U}'\tilde{\boldsymbol{p}}'_{\mathrm{x}_2})^{\mathrm{T}}; \dots; (\boldsymbol{V}'\boldsymbol{U}'\tilde{\boldsymbol{p}}'_{\mathrm{x}_{N_{\mathrm{u}}}})^{\mathrm{T}}\right], \tag{5-2}$$

with

$$\tilde{\boldsymbol{p}}'_{\mathrm{x}_k} = \left[\tilde{\boldsymbol{p}}^{\mathrm{T}}_{\mathrm{x}_{k_{l-1}}}, \boldsymbol{0}^{\mathrm{T}}_{C_g}, \tilde{\boldsymbol{p}}^{\mathrm{T}}_{\mathrm{x}_{k_l}}, \boldsymbol{0}^{\mathrm{T}}_{C_g}, \tilde{\boldsymbol{p}}^{\mathrm{T}}_{\mathrm{x}_{k_{l+1}}}\right]^{\mathrm{T}}_{(3N_{\mathrm{q}}+2C_g)}, \tag{5-3}$$

$\boldsymbol{V}'$ is an extension of the matrix (3-9) with dimensions $N_{\mathrm{tot}} \times (3N_{\mathrm{q}} + 2C_g - 1)M + 1$ and $\boldsymbol{U}'$ is constructed analogously to (3-8) with size $(3N_{\mathrm{q}} +$

$2C_g - 1)M + 1 \times (3N_q + 2C_g)$.

The detection process for $\tilde{\boldsymbol{z}}_l$ is executed as was explained in Section 4.2.4. Given the considered side lobes size, each block is disturbed by up to N_{tot} samples from the previous and subsequent block, respectively. Fig. 5.2 shows the BER performance considering IBI with the impact of the guard interval.

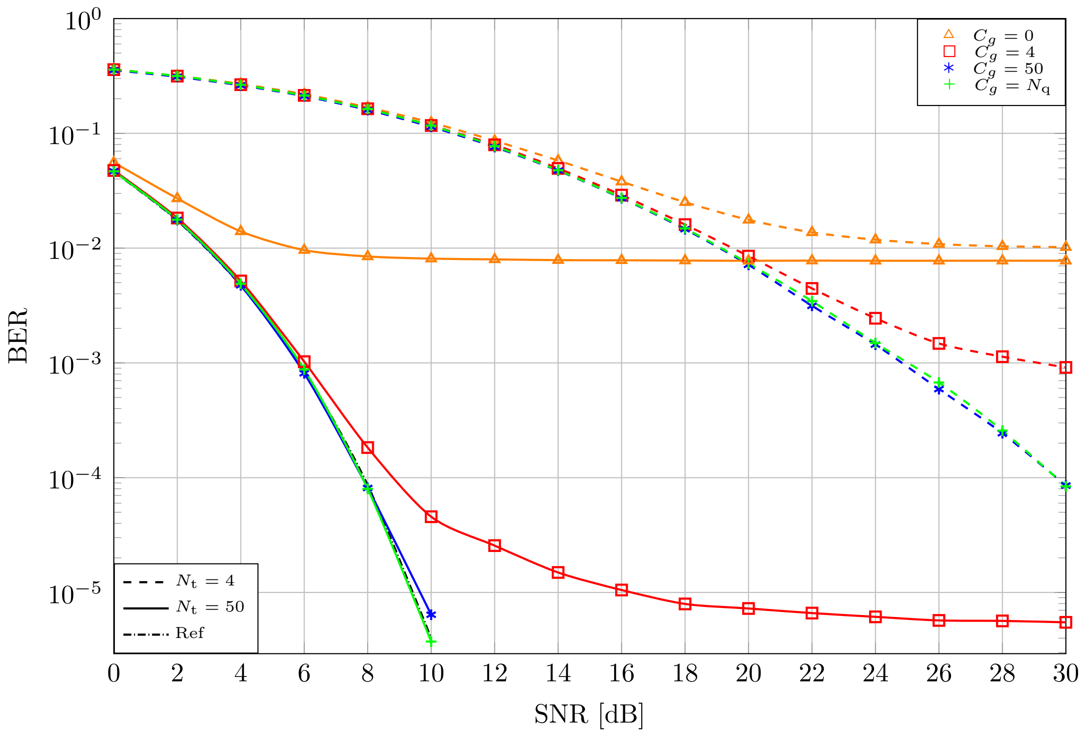

Figure 5.1: BER vs SNR considering IBI and different values of guard interval (C_g). The curves are shown for $N_t = 50$, $N_u = 5$ and $N_t = 4$, $N_u = 2$. Where Ref refers to $M_{\text{Rx}} = 2$, $M_{\text{Tx}} = 2$ with $N_t = 50$ (without IBI)

The simulation results show that a short guard time interval between the transmission blocks is sufficient to decrease considerably the effects of IBI for achieving a better performance in terms of a lower BER.

5.2 MMSE IBI

As for the case with the MMDDT IBI it is considered the transmission of L blocks, the received signal including IBI reads

$$\begin{aligned}\tilde{\boldsymbol{z}} =& Q_1\left(\tilde{\boldsymbol{y}}\right)\\ =& Q_1\left(\left(\tilde{\boldsymbol{H}} \otimes \boldsymbol{I}_{N_{\text{tot}}}\right)\left(\boldsymbol{I}_{N_t} \otimes \boldsymbol{V}'\boldsymbol{U}'\right)\tilde{\boldsymbol{p}}_{\text{x}_{\text{IBI}}} + \left(\boldsymbol{I}_{N_u} \otimes \boldsymbol{G}_{\text{Rx}}\right)\tilde{\boldsymbol{n}}\right),\end{aligned} \quad (5\text{-}4)$$

where

$$\tilde{\boldsymbol{p}}_{\mathrm{xIBI}} = \left[\tilde{\boldsymbol{p}}'^{\mathrm{T}}_{\mathrm{x}_1}, \cdots, \tilde{\boldsymbol{p}}'^{\mathrm{T}}_{\mathrm{x}_k}, \cdots, \tilde{\boldsymbol{p}}'^{\mathrm{T}}_{\mathrm{x}_{N_\mathrm{u}}}\right]^{\mathrm{T}}_{(3N_\mathrm{q}+2C_g)N_\mathrm{u}}, \tag{5-5}$$

$$\tilde{\boldsymbol{p}}'_{\mathrm{x}_k} = \left[\tilde{\boldsymbol{p}}^{\mathrm{T}}_{\mathrm{x}_{k_{l-1}}}, \mathbf{0}^{\mathrm{T}}_{C_g}, \tilde{\boldsymbol{p}}^{\mathrm{T}}_{\mathrm{x}_{k_l}}, \mathbf{0}^{\mathrm{T}}_{C_g}, \tilde{\boldsymbol{p}}^{\mathrm{T}}_{\mathrm{x}_{k_{l+1}}}\right]^{\mathrm{T}}_{(3N_\mathrm{q}+2C_g)}, \tag{5-6}$$

$\boldsymbol{V}'$ is an extension of the matrix (3-9) with dimensions $N_{\mathrm{tot}} \times (3N_\mathrm{q} + 2C_g - 1)M + 1$ and $\boldsymbol{U}'$ is constructed analog to (3-8) with size $(3N_\mathrm{q} + 2C_g - 1)M + 1 \times (3N_\mathrm{q} + 2C_g)$.

The detection process for $\tilde{\boldsymbol{z}}$ is executed as was explained in Section 4.3.2. Given the considered side lobes size, each block is disturbed by up to N_{tot} samples from the previous and subsequent block, respectively. Fig. 5.2 shows the BER performance considering IBI with the impact of the guard interval.

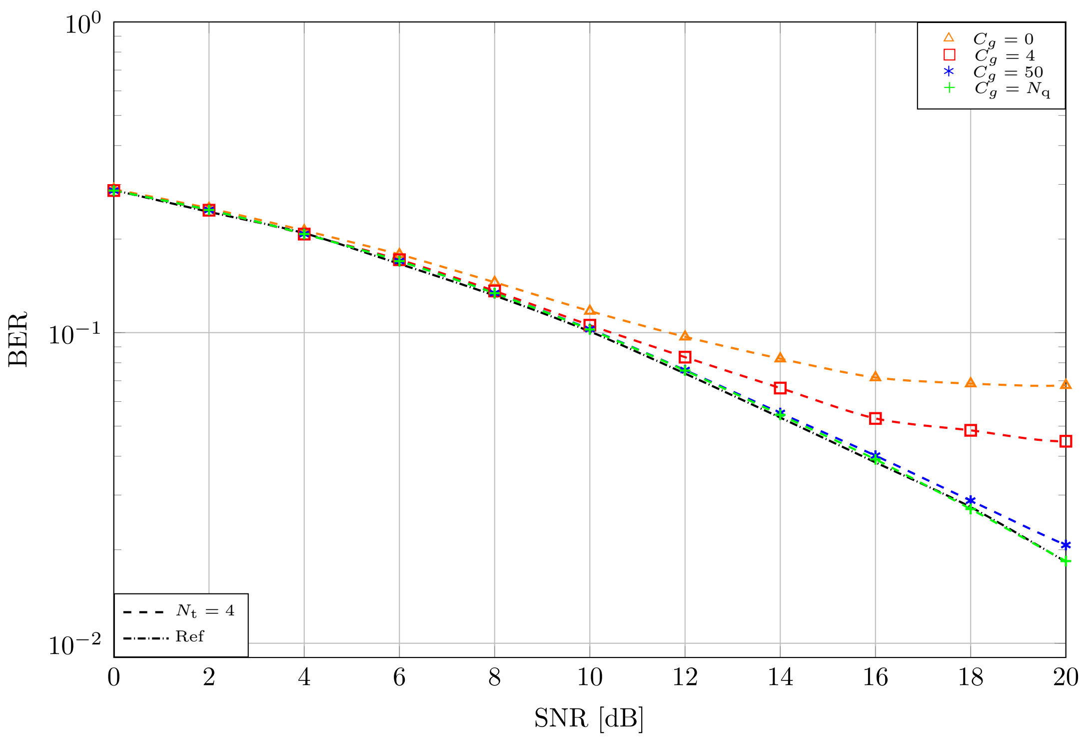

Figure 5.2: BER vs SNR considering IBI and different values of guard interval (C_g). The curves are shown for $N_\mathrm{t} = 4$, $N_\mathrm{u} = 2$. Where Ref refers to $M_{\mathrm{Rx}} = 2$, $M_{\mathrm{Tx}} = 2$ without IBI

The simulation results show that a short guard time interval between the transmission blocks is sufficient to decrease considerably the effects of IBI for achieving a better performance in terms of a lower BER.

6
Discussion

In this section the MMDDT precoder and MMSE precoder based on zero-crossing modulation described in Chapter 4 for systems employing 1-bit quantization and oversampling are summarized. Furthermore, the comparison between the precoders mentioned above and with the state-of-the-art [11] are discussed.

6.1
Performance comparison

The results of the numerical evaluations carried out show a great advantage of the zero-crossing modulation which conveys the information in the time instance of the zero-crossing, with respect to the state-of-the-art presented in [11] where the optimization of γ is done through the exhaustive search of the best codebook that reaches the maximum distance to the decision threshold.

For the precoders based on zero-crossing modulation developed in this work, the performance is considerably better than the FM approach from [11]. The results shown that the temporal MMDDT design criterion with ZF spatial precoding reached a greater value of γ than the FM approach with ZF spatial precoding of [11]. On the other hand, the proposed spatial-temporal MMSE precoding with zero-crossing modulation achieved a lower MSE value than MMSE precoding developed with the FM approach from [11].

To observe more clearly the differences between the mapping strategies, zero-crossing modulation and FM approach [11], Fig. 6.1 shows an example where the transmit and receive filter still provide sufficient bandwidth and the minimum amplitude of the signal, γ is only limited by the energy constraint. The example shows the real part of the waveform $y(t)$ in a noiseless environment and the construction of $\boldsymbol{c}_{\text{out}}$ with $M_{\text{Rx}} = 3$.

The assignments corresponding to $\boldsymbol{c}_{\text{map}}$ are given in Fig. 6.2. While the assignment for the zero-crossing approach is unique and known at the receiver, for the FM approach one codebook is randomly chosen from among the 1680 possible codebooks that generate an oversampling factor of $M_{\text{Rx}} = 3$.

From Fig. 6.1 it can be seen that the sequence $\boldsymbol{c}_{\text{out}}$ constructed with zero-crossing modulation involves significantly less zero-crossings than the sequence

$\boldsymbol{c}_{\text{out}}$ constructed with the forward mapping approach from [11], relaxing the waveform $y(t)$. The numerical results that were presented in Section 4.2.5 and Section 4.3.3 show the impact of bandlimitation on the optimization problem in terms of γ and MSE for both mapping strategies. As studied in [3] less zero-crossings implies a relaxation and is relevant in the context of bandlimitation.

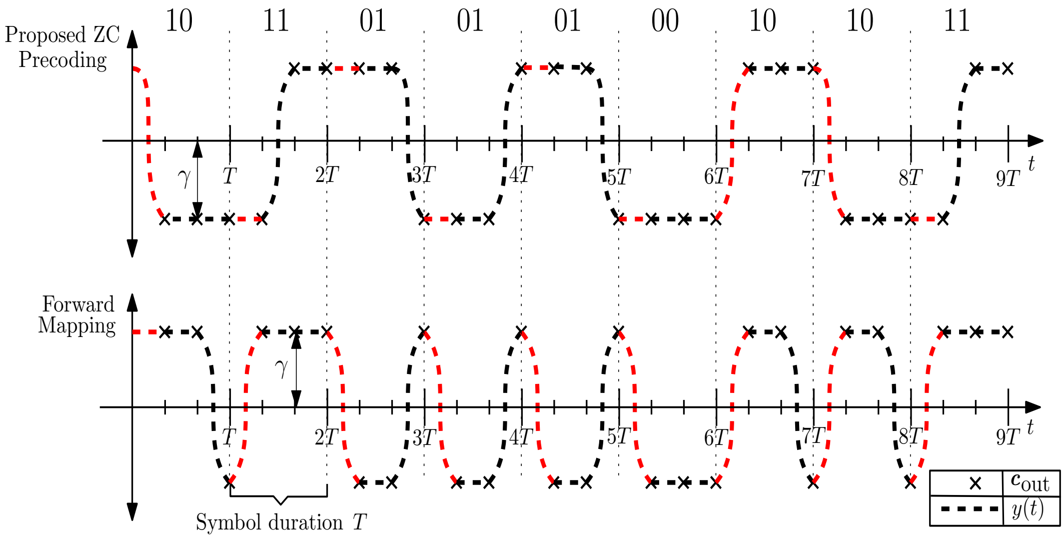

Figure 6.1: Mapping process for construction of $\boldsymbol{c}_{\text{out}}$ for ZC-precoding and an example mapping for Q-Precoding [11], $M_{\text{Rx}} = 3$

Fig. 6.3 shows a comparison, in terms of BER, of the design strategies considered in this work. On one hand, the FM approach from [11] used with the temporal MMDDT and spatial ZF precoding and with the proposed space-time MMSE precoding is shown. Along with these curves, the temporal MMDDT and spatial ZF precoding design and the proposed space-time MMSE precoding developed with novel zero-crossing method is also shown.

The results, as already stated in Fig. 4.4 and Fig. 4.8, show a better performance with the zero-crossing approach. Between both precoders studied and for both approaches (ZC and FM [11]) the MMSE space-time precoding has a better performance, in terms of BER, for low SNR.

The precoders: temporal MMDDT with spatial ZF and the space-time MMSE precoding are compared under the effects of IBI with the proposed zero-crossing approach. As can be seen in Fig. 6.4 the space-time MMSE precoding has a better performance for low SNR and the guard time interval still remains as an important factor to reduce the distortion caused by the IBI effect

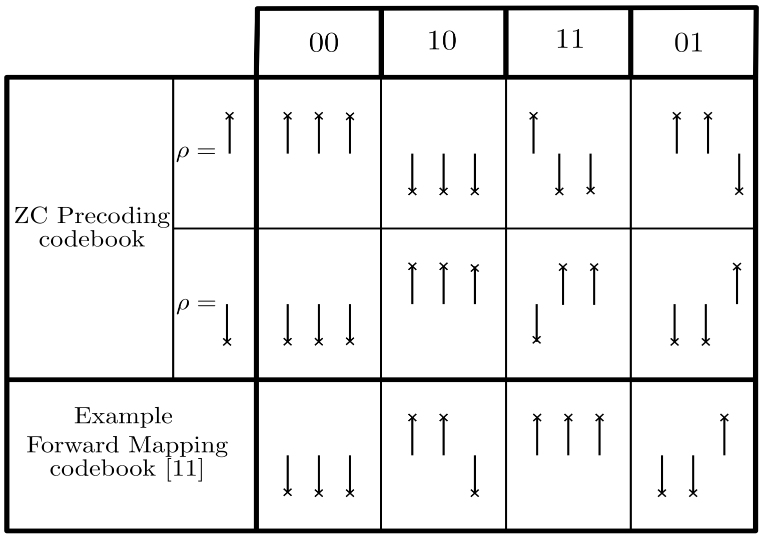

Figure 6.2: Mapping assignment for the example of Fig. 6.1

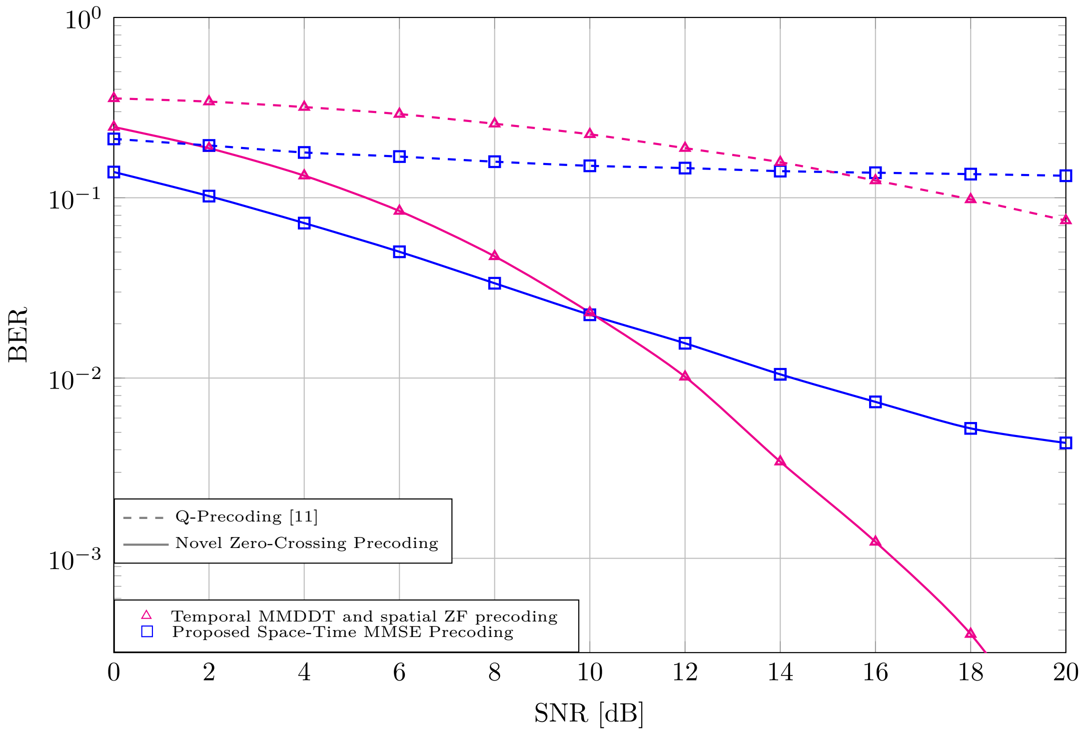

Figure 6.3: Comparison between different precoding design criteria: proposed space-time MMSE precoding design versus the temporal MMDDT and spatial ZF precoding design. Comparison between precoding strategies: Novel Zero-Crossing method versus the dynamic optimization based forward mapping [11]. ($M_{\mathrm{Rx}} = M_{\mathrm{Tx}} = 2$ with $N = 50$, $N_{\mathrm{t}} = 10$ and $N_{\mathrm{u}} = 2$)

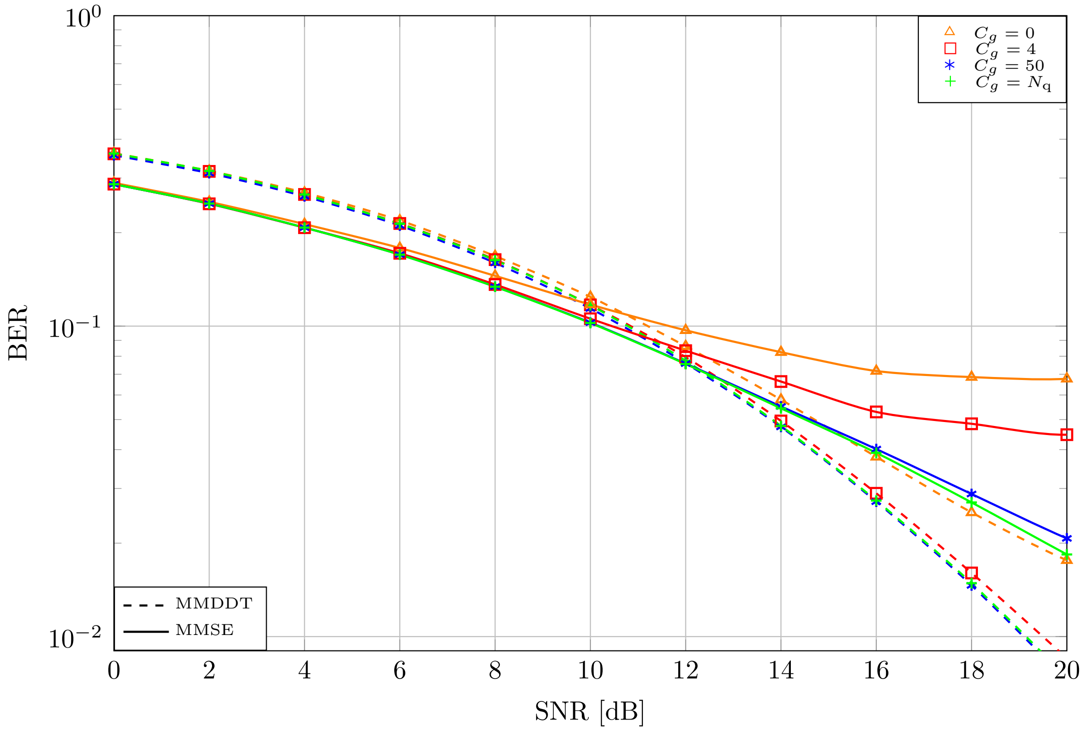

Figure 6.4: Comparison between temporal MMDDT with spatial ZF and the space-time MMSE precoding under the IBI effects with different values of guard interval (C_g). The curves are shown for $N_\mathrm{t} = 4$, $N_\mathrm{u} = 2$.

7
Conclusions

In this work we have proposed two different precoders for systems with 1-bit quantization and oversampling at the receivers. The novelty in this work is the zero-crossing modulation that has been implemented which takes advantage of the oversampling such that the information is conveyed in the time instant of zero-crossings of the received signal.

Together with the novel zero-crossing modulation, it was also implemented a bit mapping scheme which extends the principle idea behind the Gray-code to the proposed zero-crossing modulation to further improve the BER.

The waveform design scheme is tailored to applications that require low power consumption at the receivers as in IoT systems. In order to meet this requirements, a detection process was implemented that allows for a very low complexity symbol detection suitable for receivers with 1-bit quantization and oversampling. According to the zero-crossing modulation, the Hamming distance metric was used as it was suggested in the literature. This detection process requires a memory, in terms of one sample which improves the system performance without significantly increasing the detector complexity.

The novel approach of zero-crossing modulation was devised together with a MMDDT temporal precoding with spatial precoder zero forcing and also was devised with a joint space-time MMSE precoding design.

The MMDDT temporal precoding optimizes the waveform design through the maximization of the minimum distance to the decision threshold of the received signal and is implemented together with the spatial ZF precoder, that provides a beamforming gain which increases the noise tolerance as the number of transmit antennas increases. The space-time MMSE precoding design, on the other hand, optimizes the waveform design with the minimization of the error between the received signal and the desired sample pattern at the receiver.

Experiments were carried out for different values of M_{Rx} and M_{Tx} using both precoders with the zero-crossing modulation approach. The results showed that $M_{\mathrm{Rx}} = M_{\mathrm{Tx}} = 2$ is the configuration that presents the best performance in terms of BER. This results also show a trade-off, in terms of performance, between FTN and oversampling since a value of $M_{\text{Rx}} > 2$ implies a larger number of zero-crossings and $M_{\text{Tx}} > 1$ represents a benefit in the sense that it provides more degrees of freedom which can be exploited for sequence optimization.

The zero crossing modulation approach proposed in this work was compared with the state-of-the art method of forward mapping from [11]. Both modulation approaches were implemented under the same experimental conditions together with the MMDDT time with spatial ZF precoding and the space-time MMSE precoding. The results show a remarkable difference between the performance of both approaches, being the zero-crossing modulation the one which presents the best performance for both precoders performed. In addition, as it was shown in Table 4.3, FM shows a larger number of zero-crossings which implies greater complexity for the waveform design optimization.

Another advantage of the zero-crossing modulation with respect to FM is that FM needs to perform a dynamic search of the best codebook among all the existing codebooks for a given oversampling value. This dynamic search is performed by solving the optimization problem for each user and for each transmitted sequence, which implies an increase in the computational complexity and in the use of additional resources to send the information about the selected codebook.

In the case of zero-crossing modulation the zero-crossing assignment is unique and known at the receiver which implies that it is not necessary to use additional resources to transmit said information. Moreover the waveform design optimization process is performed only once per sequence and per user, saving band resources and decreasing the computational complexity.

Experiments were also carried out under the influence of the bandwidth for both approaches and with both precoders. The results shown that for the MMDDT temporal precoding with ZF γ tends to grow with the increase in bandwidth until it is limited only by the total transmit energy constraint. In this point both, FM and ZC modulation approaches reach the same value of γ and on the other hand when the bandwidth decreases, γ tends to zero. However, in real systems where bandlimitations exist, the ZC modulation provides a larger distance to the decision threshold.

For the space-time MMSE precoding, the experimental results in which the effect of bandwidth on MSE was studied showed that the MSE tends to decrease with the increase of the bandwidth. the results also showed that for both approaches, the zero-crossing precoding and the FM mapping from [11] tend to a similar value of MSE when the W_{Tx} goes to infinity. However, when the bandwidth is constrained as in the real cases, the proposed zero-crossing modulation approach corresponds to a significantly lower MSE than the FM approach devised in [11].

Finally, the two precoders and both approaches were compared together in terms of BER, with the space-time MMSE precoding presenting the best performance for low SNR and the MMDDT temporal precoding with ZF the one which has the best performance for high signal-to-noise ratio values.

The issues open to work even with 1-bit receivers are now under discussion. Based on the observations of the simulation results, the zero-crossing modulation provides a wide range of future works to develop. Just the same as the MMSE precoder that was developed together in space and time, the MMDDT precoder could be optimized taking into account the spatial precoding within its objective function. Finally it could be also of great interest to develop the performance analysis of the precoders with low resolution quantizers with more than 1-bit and including of course zero-crossing modulation.

Bibliography

[1] J. CHEN AND L. ZHANG AND Y. LIANG AND X. KANG AND R. ZHANG. **Resource allocation for wireless-powered IoT networks with short packet communication**. IEEE Trans. Commun., 18(2):1447–1461, 2019.

[2] A. GUPTA AND R. K. JHA. **A survey of 5G network: Architecture and emerging technologies**. IEEE Access, 3:1206–1232, 2015.

[3] SHAMAI (SHITZ), S. . **Information rates by oversampling the sign of a bandlimited process**. IEEE Trans. Inf. Theory, 40:1230–1236, July 1994.

[4] KOCH, T. AND LAPIDOTH, A.. **Increased capacity per unit-cost by oversampling**. In: PROC. OF THE IEEE CONVENTION OF ELECTRICAL AND ELECTRONICS ENGINEERS IN ISRAEL, Eilat, Israel, Nov. 2010.

[5] LANDAU, L. AND DÖRPINGHAUS, M. AND FETTWEIS, G. P.. **1-bit quantization and oversampling at the receiver: Communication over bandlimited channels with noise**. IEEE Commun. Lett., 21:1007–1010, 2017.

[6] LANDAU, L. AND KRONE, S. AND FETTWEIS, G. P.. **Intersymbol-interference design for maximum information rates with 1-bit quantization and oversampling at the receiver**. In: PROC. OF THE INT. ITG CONF. ON SYSTEMS, COMMUNICATIONS AND CODING, Munich, Germany, Jan 2013.

[7] L. T. N. LANDAU AND R. C. DE LAMARE. **Branch-and-bound precoding for multiuser MIMO systems with 1-bit quantization**. IEEE Wireless Communications Letters, 6:770–773, Dec 2017.

[8] MO, J. AND HEATH JR, R. W.. **Capacity analysis of one-bit quantized MIMO systems with transmitter channel state information**. IEEE Trans. Signal Process., 63:5498–5512, Oct 2015.

[9] H. JEDDA AND A. MEZGHANI AND A. L. SWINDLEHURST AND J. A. NOSSEK. **Quantized constant envelope precoding with PSK and QAM signaling**. IEEE Trans. Wireless Commun., 17:8022–8034, Dec 2018.

[10] GOKCEOGLU, A. AND BJÖRNSON, E. AND LARSSON, E. G. AND VALKAMA, M.. **Waveform design for massive MISO downlink with energy-efficient receivers adopting 1-bit ADCs**. In: IEEE INT. CONF. COMMUN., Kuala Lumpur, Malaysia, May 2016.

[11] A. GOKCEOGLU AND E. BJÖRNSON AND E. G. LARSSON AND M. VALKAMA. **Spatio-temporal waveform design for multiuser massive MIMO downlink with 1-bit receivers**. IEEE J. Sel. Topics Signal Process., 11(2):347–362, March 2017.

[12] T.S RAPPAPORT, R.W. HEATH JR, R.C. DANIELS AND J.N . MURDOCK. **Millimeter wave wireless communications**. In: COMPUTER SCIENCEELECTRICAL AND COMPUTER ENGINEERING, 2015.

[13] ALAN J. L E . **Characterization of bandimited functions and processes**. In: INFORMATION AND CONTROL (1976), p. 258–271, 1976.

[14] G. SINGH AND L. LANDAU AND G. FETTWEIS. **Finite length reconstructible ask-sequences received with 1-bit quantization and oversampling**. In: SCC 2015; 10TH INTERNATIONAL ITG CONFERENCE ON SYSTEMS, COMMUNICATIONS AND CODING, p. 1–6, Feb 2015.

[15] J. E. MAZO. **Faster-than-nyquist signaling**. The Bell System Technical Journal, 54(8):1451–1462, Oct 1975.

[16] EZIO BIGLIERI ; ANTHONY CONSTANTINIDES; ANDREA GOLDSMITH; AROGYASWAMI PAULRAJ; H. VINCENT POOR. **MIMO Wireless Communications**. Cambridge University Press, 21st edition, 2009.

[17] H. Q. NGO AND E. G. LARSSON AND T. L. MARZETTA. **Energy and spectral efficiency of very large multiuser MIMO systems**. IEEE Trans. Commun., p. 1436–1449, April 2013.

[18] LANDAU, L. AND KRONE, S. AND FETTWEIS, G. P.. **Intersymbol-interference design for maximum information rates with 1-bit quantization and oversampling at the receiver**. In: PROC. OF THE INT. ITG CONF. ON SYSTEMS, COMMUNICATIONS AND CODING, Munich, Germany, Jan 2013.

[19] BOYD, S. AND VANDENBERGHE, L.. **Convex Optimization**. Cambridge University Press, New York, NY, USA, 2004.

[20] Q. H. SPENCER AND A. L. SWINDLEHURST AND M. HAARDT. **Zero-forcing methods for downlink spatial multiplexing in multiuser MIMO channels**. IEEE Trans. Signal Process., p. 461–471, Feb 2004.

[21] M. JOHAM AND W. UTSCHICK AND J. A. NOSSEK. **Linear transmit processing in mimo communications systems**. IEEE Transactions on Signal Processing, p. 2700–2712, Aug 2005.

[22] MICHAEL JOHAM. **MIMO Systems**. Associate Institute for Signal Processing, Munich, 2010.

A
Derivation of ZF precoding matrix

Assuming
$$\begin{aligned}\hat{\tilde{\boldsymbol{P}}}_{\mathrm{x}} &= f(\tilde{\boldsymbol{H}}\tilde{\boldsymbol{P}}\tilde{\boldsymbol{P}}_{\mathrm{x}} + \tilde{\boldsymbol{N}}) \\ \mathbb{E}\left[\tilde{\boldsymbol{P}}_{\mathrm{x,Tx}}\tilde{\boldsymbol{P}}^{\mathrm{H}}_{\mathrm{x,Tx}}\right] &= \boldsymbol{C}_{\mathrm{x}} \\ \mathbb{E}\left[\tilde{\boldsymbol{N}}\tilde{\boldsymbol{N}}^{\mathrm{H}}\right] &= \boldsymbol{C}_{\mathrm{n}},\end{aligned} \tag{A-1}$$
the zero-forcing precoding problem can be expressed as
$$\begin{aligned}\left\{\tilde{\boldsymbol{P}}_{\mathrm{zf}}, f_{\mathrm{zf}}\right\} &= \arg\min_{\tilde{\boldsymbol{P}},f} \mathbb{E}\left[\left\|\hat{\tilde{\boldsymbol{P}}}_{\mathrm{x}} - \tilde{\boldsymbol{P}}_{\mathrm{x}}\right\|_F^2\right] \\ &\text{subject to:} \quad \mathbb{E}\left[\hat{\tilde{\boldsymbol{P}}}_{\mathrm{x}} \mid \tilde{\boldsymbol{P}}_{\mathrm{x}}\right] = \tilde{\boldsymbol{P}}_{\mathrm{x}}.\end{aligned} \tag{A-2}$$
From the design criterion of unbiasedness
$$\mathbb{E}\left[\hat{\tilde{\boldsymbol{P}}}_{\mathrm{x}} \mid \tilde{\boldsymbol{P}}_{\mathrm{x}}\right] = f\tilde{\boldsymbol{H}}\tilde{\boldsymbol{P}}\tilde{\boldsymbol{P}}_{\mathrm{x}} = \tilde{\boldsymbol{P}}_{\mathrm{x}}, \tag{A-3}$$
the ZF constraint can be equivalently described by
$$f\tilde{\boldsymbol{H}}\tilde{\boldsymbol{P}} = \boldsymbol{I}. \tag{A-4}$$
As the power constraint yields $\mathrm{trace}\left\{\tilde{\boldsymbol{P}}\boldsymbol{C}_{\mathrm{x}}\tilde{\boldsymbol{P}}\right\} = E_0$, then the MSE is only related to the noise as follow
$$\begin{aligned}\tilde{\boldsymbol{P}}_{\mathrm{zf}} = \arg\min_{\tilde{\boldsymbol{P}},\boldsymbol{f}} \quad & \mathbb{E}\left[\left\|-f\tilde{\boldsymbol{N}}\right\|_F^2\right] = f^2\mathrm{trace}\left\{\boldsymbol{C}_{\mathrm{n}}\right\} \\ \text{subject to:} \quad & f\tilde{\boldsymbol{H}}\tilde{\boldsymbol{P}} = \boldsymbol{I} \\ & \mathrm{trace}\left\{\tilde{\boldsymbol{P}}\boldsymbol{C}_{\mathrm{x}}\tilde{\boldsymbol{P}}\right\} = E_0.\end{aligned} \tag{A-5}$$
The Lagrangian function is formed as

$$\begin{aligned}L\left(\tilde{\boldsymbol{P}}, f, \Delta, \lambda\right) =& f^2\mathrm{trace}\left\{\boldsymbol{C}_{\mathrm{n}}\right\} + \frac{1}{2}\mathrm{trace}\left\{\Delta(f\tilde{\boldsymbol{H}}\tilde{\boldsymbol{P}} - \boldsymbol{I})\right\} \\ &+ \frac{1}{2}\mathrm{trace}\left\{\Delta(f\tilde{\boldsymbol{H}}^{\mathrm{H}}\Delta^{\mathrm{H}}\tilde{\boldsymbol{P}}^{\mathrm{H}})\right\} \\ &- \mathrm{trace}\left\{\Delta^{\mathrm{H}}\right\} + \lambda\left(\mathrm{trace}\left\{\tilde{\boldsymbol{P}}\boldsymbol{C}_{\mathrm{x}}\tilde{\boldsymbol{P}}^{\mathrm{H}}\right\}\right).\end{aligned} \tag{A-6}$$

The KKT conditions read as
$$\frac{\partial L\left(\tilde{\boldsymbol{P}}, f, \Delta, \lambda\right)}{\partial \tilde{\boldsymbol{P}}^*} = \frac{f}{2}\tilde{\boldsymbol{H}}^{\mathrm{H}}\Delta^{\mathrm{H}} + \lambda\tilde{\boldsymbol{P}}\boldsymbol{C}_{\mathrm{x}} = \boldsymbol{0}. \tag{A-7}$$
Rearranging (A-7) yields

$$\tilde{\boldsymbol{P}} = \frac{-f}{2\lambda}\tilde{\boldsymbol{H}}^{\mathrm{H}}\Delta^{\mathrm{H}}\boldsymbol{C}_{\mathrm{x}}^{-1}. \tag{A-8}$$

Replacing (A-8) in the ZF constraint (A-4) yields

$$\begin{aligned} f\tilde{\boldsymbol{H}}\left(\frac{-f}{2\lambda}\tilde{\boldsymbol{H}}^{\mathrm{H}}\Delta^{\mathrm{H}}\boldsymbol{C}_{\mathrm{x}}^{-1}\right) &= \boldsymbol{I} \\ \Delta^{\mathrm{H}} &= \frac{-2\lambda}{f^2}\left(\tilde{\boldsymbol{H}}\tilde{\boldsymbol{H}}^{\mathrm{H}}\right)^{-1}\boldsymbol{C}_{\mathrm{x}}. \end{aligned} \tag{A-9}$$

By replacing (A-9) in (A-8) we have

$$\tilde{\boldsymbol{P}}_{\mathrm{sp}} = \tilde{\boldsymbol{P}}_{\mathrm{zf}} = c_{\mathrm{zf}}\tilde{\boldsymbol{H}}^{\mathrm{H}}\left(\tilde{\boldsymbol{H}}\tilde{\boldsymbol{H}}^{\mathrm{H}}\right)^{-1}. \tag{A-10}$$

The scaling factor c_{zf} is solved by replacing (A-10) into the power constraint from (A-5)

$$\operatorname{trace}\left\{c_{\mathrm{zf}}\tilde{\boldsymbol{H}}^{\mathrm{H}}\left(\tilde{\boldsymbol{H}}\tilde{\boldsymbol{H}}^{\mathrm{H}}\right)^{-1}\boldsymbol{C}_{\mathrm{x}}\left[c_{\mathrm{zf}}\tilde{\boldsymbol{H}}^{\mathrm{H}}\left(\tilde{\boldsymbol{H}}\tilde{\boldsymbol{H}}^{\mathrm{H}}\right)^{-1}\right]^{\mathrm{H}}\right\} = E_0, \tag{A-11}$$

$$c_{\mathrm{zf}}^2\operatorname{trace}\left\{\tilde{\boldsymbol{H}}^{\mathrm{H}}\left(\tilde{\boldsymbol{H}}\tilde{\boldsymbol{H}}^{\mathrm{H}}\right)^{-1}\boldsymbol{C}_{\mathrm{x}}\left[\tilde{\boldsymbol{H}}^{\mathrm{H}}\left(\tilde{\boldsymbol{H}}\tilde{\boldsymbol{H}}^{\mathrm{H}}\right)^{-1}\right]^{\mathrm{H}}\right\} = E_0. \tag{A-12}$$

Since $\boldsymbol{C}_{\mathrm{x}}$ is given by (4-9) and $\frac{E_0}{E_{\mathrm{Tx}}} = N_{\mathrm{u}}$ (A-12) yields

$$c_{\mathrm{zf}} = \sqrt{\frac{E_0}{E_{\mathrm{Tx}}\operatorname{trace}\left(\left(\tilde{\boldsymbol{H}}\tilde{\boldsymbol{H}}^{\mathrm{H}}\right)^{-1}\right)}}, \tag{A-13}$$

$$c_{\mathrm{zf}} = \sqrt{\frac{N_{\mathrm{u}}}{\operatorname{trace}\left(\left(\tilde{\boldsymbol{H}}\tilde{\boldsymbol{H}}^{\mathrm{H}}\right)^{-1}\right)}}. \tag{A-14}$$

B
Derivation of the space-time MMSE precoding

The space-time MMSE precoder derivation can be done as is suggested in [21]. The noise covariance matrix is $\boldsymbol{C}_n = \mathbb{E}\left[\tilde{\boldsymbol{n}}\tilde{\boldsymbol{n}}^H\right]$. Since the total transmit energy E_0 is constrained it is considered that the factor f scales the receive signal, so it is part of the optimization problem. Given the receive signal (4-19) and the desired output pattern $\tilde{\boldsymbol{c}}_{\mathrm{out}}$, the MMSE precoding problem can be cast as

$$\min_{f,\tilde{\boldsymbol{p}}_{\mathrm{x}}} \quad \mathrm{E}\{\|f(\tilde{\boldsymbol{H}}_{\mathrm{eff}}\tilde{\boldsymbol{p}}_{\mathrm{x}} + \boldsymbol{G}_{\mathrm{Rx,eff}}\tilde{\boldsymbol{n}}) - \tilde{\boldsymbol{c}}_{\mathrm{out}}\|_2^2\} \tag{B-1}$$

$$\text{subject to:} \quad \tilde{\boldsymbol{p}}_{\mathrm{x}}^H\boldsymbol{A}^H\boldsymbol{A}\tilde{\boldsymbol{p}}_{\mathrm{x}} \leq E_0. \tag{B-2}$$

The equivalent cost function is given by

$$\begin{aligned} J =& f^2\tilde{\boldsymbol{p}}_{\mathrm{x}}^H\tilde{\boldsymbol{H}}_{\mathrm{eff}}^H\tilde{\boldsymbol{H}}_{\mathrm{eff}}\tilde{\boldsymbol{p}}_{\mathrm{x}} - 2f\mathrm{Re}\{\tilde{\boldsymbol{p}}_{\mathrm{x}}^H\tilde{\boldsymbol{H}}_{\mathrm{eff}}^H\tilde{\boldsymbol{c}}_{\mathrm{out}}\} \\ &+ f^2\mathrm{trace}\{\boldsymbol{G}_{\mathrm{Rx,eff}}\boldsymbol{C}_n\boldsymbol{G}_{\mathrm{Rx,eff}}{}^H\}. \end{aligned} \tag{B-3}$$

With this, the Lagrangian function reads as

$$\begin{aligned} L(\tilde{\boldsymbol{p}}_{\mathrm{x}}, f, \lambda) =& f^2\tilde{\boldsymbol{p}}_{\mathrm{x}}^H\tilde{\boldsymbol{H}}_{\mathrm{eff}}^H\tilde{\boldsymbol{H}}_{\mathrm{eff}}\tilde{\boldsymbol{p}}_{\mathrm{x}} - 2f\mathrm{Re}\{\tilde{\boldsymbol{p}}_{\mathrm{x}}^H\tilde{\boldsymbol{H}}_{\mathrm{eff}}^H\tilde{\boldsymbol{c}}_{\mathrm{out}}\} \\ &+ f^2\mathrm{trace}\{\boldsymbol{G}_{\mathrm{Rx,eff}}\boldsymbol{C}_n\boldsymbol{G}_{\mathrm{Rx,eff}}{}^H\} \\ &+ \lambda\left(\tilde{\boldsymbol{p}}_{\mathrm{x}}^H\boldsymbol{A}^H\boldsymbol{A}\tilde{\boldsymbol{p}}_{\mathrm{x}} - E_0\right). \end{aligned} \tag{B-4}$$

Taking the derivative w.r.t. $\tilde{\boldsymbol{p}}_{\mathrm{x}}^*$ we have

$$\frac{dL(\tilde{\boldsymbol{p}}_{\mathrm{x}}, f, \lambda)}{d\tilde{\boldsymbol{p}}_{\mathrm{x}}^*} = \left(f^2\tilde{\boldsymbol{H}}_{\mathrm{eff}}^H\tilde{\boldsymbol{H}}_{\mathrm{eff}} + \lambda\boldsymbol{A}^H\boldsymbol{A}\right)\tilde{\boldsymbol{p}}_{\mathrm{x}} - f\tilde{\boldsymbol{H}}_{\mathrm{eff}}^H\tilde{\boldsymbol{c}}_{\mathrm{out}}, \tag{B-5}$$

and equating it to zero yields

$$\tilde{\boldsymbol{p}}_{\mathrm{x,opt}} = \frac{1}{f}\left(\tilde{\boldsymbol{H}}_{\mathrm{eff}}^H\tilde{\boldsymbol{H}}_{\mathrm{eff}} + \frac{\lambda}{f^2}\boldsymbol{A}^H\boldsymbol{A}\right)^{-1}\tilde{\boldsymbol{H}}_{\mathrm{eff}}^H\tilde{\boldsymbol{c}}_{\mathrm{out}}, \tag{B-6}$$

which can also be written as

$$\frac{1}{f}\tilde{\boldsymbol{p}}_{\mathrm{x}}^{H}\tilde{\boldsymbol{H}}_{\mathrm{eff}}^{H}\tilde{\boldsymbol{c}}_{\mathrm{out}} = \tilde{\boldsymbol{p}}_{\mathrm{x}}^{H}\left(\tilde{\boldsymbol{H}}_{\mathrm{eff}}^{H}\tilde{\boldsymbol{H}}_{\mathrm{eff}} + \frac{\lambda}{f^2}\boldsymbol{A}^H\boldsymbol{A}\right)\tilde{\boldsymbol{p}}_{\mathrm{x}}. \tag{B-7}$$

The derivative of the Lagrangian function w.r.t. f reads as

$$\begin{aligned}\frac{dL(\tilde{\boldsymbol{p}}_{\mathrm{x}}, f, \lambda)}{df} =& 2f\tilde{\boldsymbol{p}}_{\mathrm{x}}^{H}\tilde{\boldsymbol{H}}_{\mathrm{eff}}^{H}\tilde{\boldsymbol{H}}_{\mathrm{eff}}\tilde{\boldsymbol{p}}_{\mathrm{x}} - 2\mathrm{Re}\{\tilde{\boldsymbol{p}}_{\mathrm{x}}^{H}\tilde{\boldsymbol{H}}_{\mathrm{eff}}^{H}\tilde{\boldsymbol{c}}_{\mathrm{out}}\} \\ &+ 2f\mathrm{trace}\{\boldsymbol{G}_{\mathrm{Rx,eff}}\boldsymbol{C}_n{\boldsymbol{G}_{\mathrm{Rx,eff}}}^H\},\end{aligned} \tag{B-8}$$

where the real part operator can be skipped because its argument is always real valued when taking into account the structure of $\tilde{\boldsymbol{p}}_{\mathrm{x,opt}}$. Equating the (B-8) to zero yields

$$\frac{1}{f}\tilde{\boldsymbol{p}}_{\mathrm{x}}^{H}\tilde{\boldsymbol{H}}_{\mathrm{eff}}^{H}\tilde{\boldsymbol{c}}_{\mathrm{out}} = \tilde{\boldsymbol{p}}_{\mathrm{x}}^{H}\tilde{\boldsymbol{H}}_{\mathrm{eff}}^{H}\tilde{\boldsymbol{H}}_{\mathrm{eff}}\tilde{\boldsymbol{p}}_{\mathrm{x}} + \mathrm{trace}\{\boldsymbol{G}_{\mathrm{Rx,eff}}\boldsymbol{C}_n{\boldsymbol{G}_{\mathrm{Rx,eff}}}^H\}. \tag{B-9}$$

Equating the RHS of (B-7) with the RHS of (B-9) gives

$$\frac{\lambda}{f^2} = \frac{\mathrm{trace}\{\boldsymbol{G}_{\mathrm{Rx,eff}}\boldsymbol{C}_n{\boldsymbol{G}_{\mathrm{Rx,eff}}}^H\}}{\tilde{\boldsymbol{p}}_{\mathrm{x}}^{H}\boldsymbol{A}^H\boldsymbol{A}\tilde{\boldsymbol{p}}_{\mathrm{x}}}. \tag{B-10}$$

Based on the fact that any precoding vector $\tilde{\boldsymbol{p}}_{\mathrm{x}}$ with less than the maximum transmit energy cannot be optimal in the MSE sense, we can consider equality for the transmit energy constraint. With this, (B-10) can be written with the maximum transmit energy as

$$\frac{\lambda}{f^2} = \frac{\mathrm{trace}\{\boldsymbol{G}_{\mathrm{Rx,eff}}\boldsymbol{C}_n{\boldsymbol{G}_{\mathrm{Rx,eff}}}^H\}}{E_0}. \tag{B-11}$$

Then the optimal precoding vector can be expressed as

$$\begin{aligned}&\tilde{\boldsymbol{p}}_{\mathrm{x,opt}} = \\ &\frac{1}{f}\left(\tilde{\boldsymbol{H}}_{\mathrm{eff}}^{H}\tilde{\boldsymbol{H}}_{\mathrm{eff}} + \frac{\mathrm{trace}\{\boldsymbol{G}_{\mathrm{Rx,eff}}\boldsymbol{C}_n{\boldsymbol{G}_{\mathrm{Rx,eff}}}^H\}}{E_0}\boldsymbol{A}^H\boldsymbol{A}\right)^{-1}\tilde{\boldsymbol{H}}_{\mathrm{eff}}^{H}\tilde{\boldsymbol{c}}_{\mathrm{out}}.\end{aligned} \tag{B-12}$$

Inserting (B-12) into the transmit energy constraint determines the scaling factor, which is then given by

$$f = \sqrt{\frac{\tilde{\boldsymbol{c}}_{\text{out}}^H \boldsymbol{\Gamma} \tilde{\boldsymbol{c}}_{\text{out}}}{E_0}}, \tag{B-13}$$

with

$$\begin{aligned}\boldsymbol{\Gamma} =& \tilde{\boldsymbol{H}}_{\text{eff}} \left(\tilde{\boldsymbol{H}}_{\text{eff}}^H \tilde{\boldsymbol{H}}_{\text{eff}} + \frac{\text{trace}\{\boldsymbol{G}_{\text{Rx,eff}} \boldsymbol{C}_n \boldsymbol{G}_{\text{Rx,eff}}{}^H\}}{E_0} \boldsymbol{A}^H \boldsymbol{A} \right)^{-1} \boldsymbol{A}^H \times \\ & \boldsymbol{A} \left(\tilde{\boldsymbol{H}}_{\text{eff}}^H \tilde{\boldsymbol{H}}_{\text{eff}} + \frac{\text{trace}\{\boldsymbol{G}_{\text{Rx,eff}} \boldsymbol{C}_n \boldsymbol{G}_{\text{Rx,eff}}{}^H\}}{E_0} \boldsymbol{A}^H \boldsymbol{A} \right)^{-1} \tilde{\boldsymbol{H}}_{\text{eff}}^H.\end{aligned} \tag{B-14}$$

C
Published papers

The paper *Zero-Crossing Precoding with Maximum Distance to the Decision Threshold for Channels With 1-Bit Quantization and Oversampling*, was presented at the International Conference on Acoustics, Speech, and Signal Processing, ICASSP 2020. The paper was accepted for presentation in a poster session at the conference on May 4-8, 2020 in Barcelona, Spain.

The paper *Zero-Crossing Precoding with MMSE Criterion for Channels With 1-Bit Quantization and Oversampling*, was presented at the 24th International ITG Workshop on Smart Antennas (WSA 2020). The paper was accepted for oral presentation on February 18-20, 2020 in Hamburg, Germany.